Eur. Phys. J. C (2020) 80:73
https://doi.org/10.1140/epjc/s10052-020-7624-4

THE EUROPEAN PHYSICAL JOURNAL C

Regular Article - Experimental Physics

Transverse momentum and process dependent azimuthal anisotropies in $\sqrt{s_{\mathrm{NN}}} = 8.16$ TeV p+Pb collisions with the ATLAS detector

ATLAS Collaboration[⋆]

CERN, 1211 Geneva 23, Switzerland

Received: 31 October 2019 / Accepted: 7 January 2020 / Published online: 30 January 2020

Abstract The azimuthal anisotropy of charged particles produced in $\sqrt{s_{\mathrm{NN}}} = 8.16$ TeV p+Pb collisions is measured with the ATLAS detector at the LHC. The data correspond to an integrated luminosity of 165 nb^{-1} that was collected in 2016. Azimuthal anisotropy coefficients, elliptic v_2 and triangular v_3, extracted using two-particle correlations with a non-flow template fit procedure, are presented as a function of particle transverse momentum (p_{T}) between 0.5 and 50 GeV. The v_2 results are also reported as a function of centrality in three different particle p_{T} intervals. The results are reported from minimum-bias events and jet-triggered events, where two jet p_{T} thresholds are used. The anisotropies for particles with p_{T} less than about 2 GeV are consistent with hydrodynamic flow expectations, while the significant non-zero anisotropies for p_{T} in the range 9–50 GeV are not explained within current theoretical frameworks. In the p_{T} range 2–9 GeV, the anisotropies are larger in minimum-bias than in jet-triggered events. Possible origins of these effects, such as the changing admixture of particles from hard scattering and the underlying event, are discussed.

1 Introduction

The collisions of heavy nuclei at relativistic speeds generate hot and dense droplets of matter composed of deconfined quarks and gluons known as the quark–gluon plasma (QGP) [1,2]. Studies of the QGP at the Relativistic Heavy Ion Collider (RHIC) and the Large Hadron Collider (LHC) have yielded a wealth of surprising results that reveal a complex set of QGP-related phenomena. Bulk hadron production, occurring mainly at low transverse momentum ($p_{\mathrm{T}} \lesssim 3$ GeV), exhibits significant azimuthal anisotropies that are well described in terms of nearly inviscid hydrodynamic flow of the QGP [1]. The final hadron momentum anisotropies arise from inhomogeneities in the initial spatial distribution of the QGP translated to momentum space via strong differential pressure gradients. These anisotropies are characterised in terms of a Fourier decomposition:

$$Y(\phi) = G\left[1 + 2\sum_{n=1}^{\infty} v_n \cos(n(\phi - \Psi_n))\right],$$

where v_n are the anisotropy coefficients, Ψ_n is the nth-order orientation of the anisotropy, and the normalization, G, is set by the integral of the distribution. In particular, v_2 and v_3 are referred to as the elliptic and triangular coefficients, respectively.

In addition, the production of high transverse momentum hadrons ($p_{\mathrm{T}} \gtrsim 10$ GeV) is highly suppressed relative to the yields expected from nuclear thickness scaling of proton–proton collision yields [3]. This suppression is understood to result from high momentum transfer parton–parton interactions followed by the outgoing partons losing energy via radiative and collisional processes in the QGP – processes referred to as jet quenching [4–6]. These high-p_{T} hadrons and associated jets are also observed to have a non-zero azimuthal anisotropy [7–9], despite being well outside the nominal domain where the anisotropies are interpreted in terms of hydrodynamic flow. Instead, these anisotropies are understood to also arise from inhomogeneities in the initial spatial distribution of the QGP, but in this case, where the jet quenching effect is stronger for partons traversing longer paths through the QGP and weaker for partons traversing shorter paths [10]. In this way, low- and high-p_{T} hadrons have a common orientation of their azimuthal anisotropy in a given event, because both are correlated with the orientation of the initial geometry of the colliding nucleons. It is notable that, for more than a decade, an outstanding and challenging theoretical puzzle has been how to quantitatively describe both high-p_{T} hadron suppression and azimuthal anisotropy in Pb+Pb collisions [11]. There are a number of proposed explanations for resolving this puzzle in heavy-ion collisions – see Refs. [12–17] for examples.

⋆ e-mail: atlas.publications@cern.ch

Measurements in smaller collision systems, pp and p+Pb collisions at the LHC [18–23] and p+Au, d+Au, and ^{3}He+Au at RHIC [24], indicate significant azimuthal anisotropies for low-p_{T} hadrons with patterns quite similar to those observed in the larger heavy-ion collision systems. For a recent review see Ref. [25]. These observations have raised the question of whether smaller and shorter-lived droplets of QGP are formed in these smaller collision systems. Indeed, models employing nearly inviscid hydrodynamics for the QGP provide a quantitative description of this large body of data at low p_{T} [26].

In contrast, measurements aimed at observing signatures of jet quenching in small collision systems have found no such effect. Measurements of hadron and jet p_{T} spectra at high p_{T} indicate production yields consistent with those in pp collisions scaled up by the expected nuclear thickness in p+Pb [27–29] and d+Au collisions [30], and that the p_{T}-balance between dijets or hadron–jet pairs is unmodified in p+Pb collisions within uncertainties [31,32]. The ATLAS experiment has also published results for the hadron azimuthal anisotropy up to $p_{\mathrm{T}} \approx 12$ GeV that hint at a non-zero anisotropy extending into the region beyond the usual hydrodynamic interpretation and into the regime of jet quenching [33]. However, it is unlikely that there can be differential jet quenching as a function of orientation relative to the QGP geometry if there is no jet quenching in p+Pb collisions as observed in the spectra. Thus, there are two related outstanding puzzles, one being the lack of jet quenching observed in the spectra, if indeed small droplets of QGP are formed, and the other being what mechanism can lead to high-p_{T} hadron anisotropies other than differential jet quenching.

This paper presents a measurement of the azimuthal anisotropy of unidentified hadrons as a function of p_{T} and centrality in $\sqrt{s_{\mathrm{NN}}} = 8.16$ TeV p+Pb collisions with the ATLAS detector. The measurement is made using two-particle correlations, measured separately for minimum-bias triggered (MBT) events and events requiring a jet with p_{T} greater than either 75 GeV or 100 GeV. There are contributions to the azimuthal correlations from particle decays, jets, dijets, and global momentum conservation, which have traditionally been referred to as 'non-flow' [34]. Using this nomenclature, a standard template fitting procedure is applied to subtract non-flow contributions [19,20]. To decrease the residual influence of the non-flow correlation in the jet events, a novel procedure is used to restrict the acceptance of particles according to the location of jets in the event. Assuming that the two-particle anisotropy coefficients are the products of the corresponding single-particle coefficients (factorisation), the elliptic and triangular anisotropy coefficients, v_2 and v_3, are reported as a function of p_{T}. Additionally, v_2 results are presented as a function of centrality in three different p_{T} ranges. Finally, the fractional contribution to the correlation functions from jet particles is determined as a function of p_{T}.

2 ATLAS detector

The ATLAS experiment [35] at the LHC is a multipurpose particle detector with a forward–backward symmetric cylindrical geometry and nearly 4π coverage.[1] This analysis relies on the inner detector, the calorimeter, and the data acquisition and trigger system.

The inner detector (ID) comprises three major subsystems: the pixel detector and the silicon microstrip tracker, which extend up to $|\eta| = 2.5$, and the transition radiation tracker, which extends to $|\eta| = 2.0$. The inner detector covers the full azimuth and is immersed in a 2 T axial magnetic field. The pixel detector consists of four cylindrical layers in the barrel region and three discs in each endcap region. A new innermost layer, the insertable B-layer [36,37], has been operating as a part of the pixel detector since 2015. The silicon microstrip tracker comprises four cylindrical layers (nine discs) of silicon strip detectors in the barrel (endcap) region. The minimum-bias trigger scintillator detects charged particles over $2.07 < |\eta| < 3.86$ using two hodoscopes of 12 counters positioned at $|z| = 3.6$ m.

The calorimeter is a large-acceptance, longitudinally segmented sampling detector covering $|\eta| < 4.9$ with electromagnetic (EM) and hadronic sections. The EM calorimeter is a lead/liquid-argon sampling calorimeter with an accordion-shaped geometry. It is divided into a barrel region, covering $|\eta| < 1.475$, and two endcap regions, covering $1.375 < |\eta| < 3.2$. The hadronic calorimeter surrounds the EM calorimeter. It consists of a steel/scintillator-tile sampling calorimeter covering $|\eta| < 1.7$ and a liquid-argon calorimeter with copper absorber covering $1.5 < |\eta| < 3.2$. The forward calorimeter (FCal) is a liquid-argon sampling calorimeter located on either side of the interaction point. It covers $3.1 < |\eta| < 4.9$ and each half is composed of one EM and two hadronic sections, with copper and tungsten serving as the absorber material, respectively. The FCal is used to characterise the centrality of p+Pb collisions as described below.

In this analysis, a two-level trigger system was used to select events, with a first-level (L1) trigger implemented in hardware followed by a software-based high-level trig-

[1] ATLAS uses a right-handed coordinate system with its origin at the nominal interaction point (IP) in the centre of the detector and the z-axis along the beam pipe. The x-axis points from the IP to the centre of the LHC ring, and the y-axis points upward. Cylindrical coordinates (r, ϕ) are used in the transverse plane, ϕ being the azimuthal angle around the z-axis. The pseudorapidity is defined in terms of the polar angle θ as $\eta = -\ln\tan(\theta/2)$. Transverse momentum and transverse energy are defined as $p_{\mathrm{T}} = p\sin\theta$ and $E_{\mathrm{T}} = E\sin\theta$, respectively. Angular distance ΔR is defined as $\sqrt{(\Delta\eta)^2 + (\Delta\phi)^2}$.

ger (HLT) which reconstructs the event in a manner similar to the final offline reconstruction. Events used for the measurements presented in this paper were selected using several triggers. MBT events were selected by a trigger that requires a signal in at least one minimum-bias trigger scintillator counter at L1 [38] followed by the requirement of at least one reconstructed track at the HLT stage. Events with a high-p_{T} jet were acquired using a high-level jet trigger covering the central region ($|\eta| < 3.2$). These events were first required to have energy deposits at L1 that are compatible with the presence of a jet and then to pass various thresholds for the jet transverse energy at the HLT stage.

3 Data and event selection

During p+Pb data-taking in 2016, the LHC was configured with a beam composed of protons with an energy of 6.5 TeV and a beam of lead ions with an energy per nucleon of 2.51 TeV. This resulted in a collision system with proton–nucleon centre-of-mass energy $\sqrt{s_{\mathrm{NN}}} = 8.16$ TeV and a rapidity shift of the centre of mass by +0.465 units in the proton-going direction relative to the laboratory frame. The data were taken over two running periods with different configurations of the LHC beam directions. In the first period of data-taking, comprising a total integrated luminosity of 57 nb^{-1}, the lead ions circulated clockwise in beam 1, while the protons circulated counterclockwise in beam 2. For the second period of data-taking, which comprised 108 nb^{-1}, the beam species were interchanged. The analysed data were provided by the minimum-bias trigger described above, which was prescaled and sampled 0.079 nb^{-1} of luminosity. In addition, data were selected by the high-level jet triggers with transverse energy thresholds of 75 GeV and 100 GeV, which sampled 26 nb^{-1} and the full 165 nb^{-1} of p+Pb luminosity, respectively.

Events selected by the triggers described above were reconstructed offline following procedures that were optimised for the Run-2 detector configuration [39]. Events are required to have at least one reconstructed vertex. To reduce the contribution from events with multiple in-time p+Pb interactions, events with more than one vertex are used only if the additional vertices have fewer than seven associated reconstructed tracks with $p_{\mathrm{T}} > 0.4$ GeV. That is, events are only allowed to have one vertex with seven or more associated tracks. Two classes of jet events were defined by requiring an offline jet with $p_{\mathrm{T}} > 75$ GeV or $p_{\mathrm{T}} > 100$ GeV respectively, and were drawn from the jet-triggered event samples with the analogous online thresholds. The trigger efficiency, given this offline selection, was greater than 97% for both jet samples.

Events were further characterised by the sum of the transverse energy in the FCal module in the direction of the Pb beam, $\Sigma E_{\mathrm{T}}^{\mathrm{Pb}}$. The event centrality is defined as the $\Sigma E_{\mathrm{T}}^{\mathrm{Pb}}$ percentile of the events in minimum-bias collisions, after accounting for the inefficiency introduced by the trigger and event selection criteria, and was determined in a way similar to previous analyses of Run-1 p+Pb data at $\sqrt{s_{\mathrm{NN}}} = 5.02$ TeV [27,40]. Events within the 0–90% centrality range were used in this analysis, with low (high) values corresponding to high-$\Sigma E_{\mathrm{T}}^{\mathrm{Pb}}$ (low-$\Sigma E_{\mathrm{T}}^{\mathrm{Pb}}$) events with large (small) overall particle multiplicity. Since the acceptance of the FCal is separate from that of the ID, this centrality definition has the benefit of reducing event-selection-induced biases in the measured quantities [41].

4 Track and jet reconstruction

The reconstruction, selection, and calibration of charged-particle tracks and calorimetric jets, and their performance as determined using Monte Carlo (MC) simulations, are described below.

Charged-particle tracks and collision vertices are reconstructed in the ID using the algorithms described in Ref. [39]. Inner detector tracks with $p_{\mathrm{T}} > 0.4$ GeV and $|\eta| < 2.5$ were required to satisfy a set of quality criteria similar to those described in Ref. [19]. The total number of reconstructed ID tracks satisfying these selection criteria in a given event is called the multiplicity or $N_{\mathrm{ch}}^{\mathrm{rec}}$. The reconstruction and selection efficiency for *primary* [42] charged hadrons to meet these criteria was determined using a sample of 3 million minimum-bias p+Pb events simulated by the HIJING generator [43]. Events were generated with both beam configurations. The ATLAS detector response to the generated events was determined through a full GEANT4 simulation [44,45], and the simulated events were reconstructed in the same way as the data. Over the measured kinematic range, the efficiency varies from approximately 50% for the lowest-p_{T} hadrons at large pseudorapidity, to greater than 90% for hadrons with $p_{\mathrm{T}} > 3$ GeV at mid-rapidity.

Jets are reconstructed using energy deposits in the calorimeter system, $|\eta| < 4.9$, in a range partially overlapping with both the ID and the FCal used to determine centrality. The reconstruction closely follows the procedure used in other measurements for Pb+Pb and pp collisions [46,47]. Jets are measured by applying the anti-k_t algorithm [48,49] with radius parameter $R = 0.4$ to energy deposits in the calorimeter. No jets with $p_{\mathrm{T}} < 15$ GeV are considered. An iterative procedure is used to obtain an event-by-event estimate of the η-dependent underlying-event energy density, while excluding jets from that estimate. The jet kinematics are corrected for this background and for the detector response using an η- and p_{T}-dependent calibration derived from fully simulated and reconstructed PYTHIA 8 [50] hard-scattering events configured with the NNPDF23LO parton distribution func-

tion set [51] and the A14 set of tuned parameters [52] to model non-perturbative effects. An additional, small correction, based on *in situ* studies of jets recoiling against photons, Z bosons, and jets in other regions of the calorimeter, is applied [53,54]. Simulation studies show that for jets with $p_{\mathrm{T}} > 75$ GeV, the average reconstructed jet p_{T} is within 1% of the generator level jet p_{T} and has a relative p_{T} resolution below 10% after the calibration procedure.

5 Analysis procedure

This analysis is based on previous ATLAS two-particle correlation studies [19,20]. To construct the two-particle correlation functions, the selected inner-detector tracks with $p_{\mathrm{T}} > 0.4$ GeV are divided into two sets, referred to as A- and B-particles in this paper, although they are sometimes referred to as trigger and associated particles in the literature. To reduce the contribution of non-flow correlations from decays and jets, two restrictions are placed on A–B particle pairs drawn from the two sets. First, as was done in previous analyses [19,20], the particles are required to be separated in pseudorapidity with $|\Delta\eta^{\mathrm{AB}}| = |\eta^{\mathrm{B}} - \eta^{\mathrm{A}}| > 2$. This requirement removes the short-range decay and jet fragmentation structure, while emphasising global, early-time correlations. Due to the enhanced contribution from jet correlations in the jet-triggered events, an additional constraint was developed for this analysis. Namely, B-particles are required to be separated in pseudorapidity by one unit from all reconstructed jets with $p_{\mathrm{T}}^{\mathrm{jet}} > 15$ GeV, i.e. $|\Delta\eta^{\mathrm{jB}}| = |\eta^{\mathrm{B}} - \eta^{\mathrm{jet}}| > 1$. This latter requirement is only applied to the jet-triggered events, and in this way, the jets act as a source of high-p_{T} A-particles but contribute few B-particles.

The correlation functions, $S(\Delta\phi)$, are defined as the yields of particle pairs passing the above event and pair selection, binned in $\Delta\phi = \phi^{\mathrm{A}} - \phi^{\mathrm{B}}$, and normalised by the total number of A-particles. Corrections for the imperfect trigger and tracking efficiencies are applied as weights to the entries of the correlation functions. A mixed-event correction, $M(\Delta\phi)$, is generated by correlating A-particles from one event with B-particles from a different event with a vertex z-position differing by less than 10 mm and a number of reconstructed charged particles ($N_{\mathrm{ch}}^{\mathrm{rec}}$) differing by less than 10 for $N_{\mathrm{ch}}^{\mathrm{rec}} < 100$ and less than 20 for $N_{\mathrm{ch}}^{\mathrm{rec}} > 100$. Thus, the mixed events contain only trivial detector acceptance effects and no physical correlations. To reduce the statistical uncertainty introduced by the correction, each event is mixed with five others meeting the above vertex z and $N_{\mathrm{ch}}^{\mathrm{rec}}$ conditions. The corrected correlation is, then, $Y(\Delta\phi) = S(\Delta\phi)/M(\Delta\phi)$, where $M(\Delta\phi)$ is normalised such that the ratio preserves the overall integral of $S(\Delta\phi)$. Jet events are mixed with other jet events, and the $|\Delta\eta^{\mathrm{jB}}|$ condition is applied with respect to the jets in the A-particle event only. Thus, the B-particle acceptance is consistent between the same- and mixed-event correlations.

To extract the anisotropy coefficients while accounting for residual non-flow, the ATLAS template fitting procedure, as used for previous results [19,20], is applied to $Y(\Delta\phi)$. In this procedure, $Y(\Delta\phi)$ is found for two different selections of event activity quantified by centrality: a central selection, $Y^{\mathrm{cent}}(\Delta\phi)$, and a peripheral selection, $Y^{\mathrm{peri}}(\Delta\phi)$. In this analysis, the peripheral selection corresponds to the 60–90% centrality interval. Assuming that the shape of the non-flow correlation is independent of centrality, $Y^{\mathrm{cent}}(\Delta\phi)$ is expressed as

$$Y^{\mathrm{cent}}(\Delta\phi) = FY^{\mathrm{peri}}(\Delta\phi) + G\left[1 + 2\sum_{n=2}^{4} v_{n,n}\cos(n\Delta\phi)\right], \quad (1)$$

where F and each $v_{n,n}$ are parameters of a global χ^2 fit, and G is fixed by the requirement that the integral of the fit model is that of Y^{cent}. The parameter F allows for a linear scaling of the non-flow between the two centrality classes. The fit includes the fourth harmonic, $v_{4,4}$, but it is not presented in the results because it is statistically insignificant. The fit χ^2 function incorporates the statistical uncertainties from both Y^{cent} and the peripheral template, Y^{peri}, although the examples shown in Figs. 1 and 2 do not show the uncertainties of Y^{peri} for readability. The statistical uncertainties of the extracted $v_{n,n}$ parameters are returned from the MINUIT χ^2 minimiser [55], accounting for correlations between parameters.

Figure 1 shows an example of two template fits using jet-triggered events with jet $p_{\mathrm{T}} > 100$ GeV. The left plot shows the fit for correlations made without the B-particle jet rejection condition, and the right plot shows the same correlation, but with the condition $|\Delta\eta^{\mathrm{jB}}| > 1$ applied. In this figure, Y_N^{ridge} represents the N^{th}-order harmonic component of the fit. The left plot has a dominant non-flow contribution, and a distortion in the resulting subtracted distribution is observed near $\Delta\phi \approx \pi$. Removing much of the jet correlation in this way reduces the overall sensitivity to the template method assumption that the shape of the non-flow contribution is the same for the central and peripheral selections. However, violation of this assumption will introduce distortions that could potentially bias the harmonic coefficients. This is explicitly tested by varying the centrality selection of the peripheral template, as discussed further in Sect. 6. Two additional examples of template fits from the jet-triggered events with jet $p_{\mathrm{T}} > 100$ GeV and with the B-particle jet rejection are plotted in Fig. 2. These show the behaviour of the template fits for high A-particle p_{T}.

If the particle momentum correlations originate from a global field, as is the case for collective expansion, the $v_{n,n}$ will factorise such that $v_{n,n}(p_{\mathrm{T}}^{\mathrm{A}}, p_{\mathrm{T}}^{\mathrm{B}}) = v_n(p_{\mathrm{T}}^{\mathrm{A}}) \cdot v_n(p_{\mathrm{T}}^{\mathrm{B}})$.

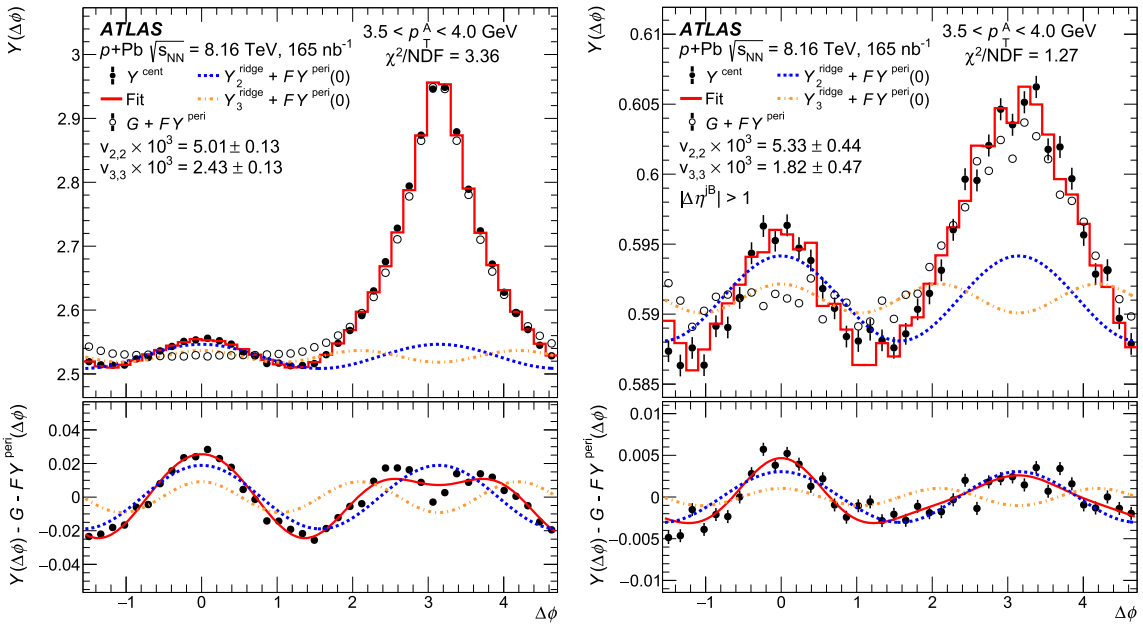

Fig. 1 Template fitting output for events with jet $p_{\mathrm{T}} > 100$ GeV. Both require $3.5 < p_{\mathrm{T}}^{\mathrm{A}} < 4.0$ GeV and are made with 60–90% peripheral selection and 0–5% central selection. The left plot is made with no selection on the B-particles and the right plot is made requiring the B-particles to have $|\Delta\eta^{\mathrm{jB}}| > 1$ relative to all jets with $p_{\mathrm{T}}^{\mathrm{jet}} > 15$ GeV in the event. In the upper panels, the open circles show the scaled and shifted peripheral template with uncertainties omitted, the closed circles show the central data, and the red line shows the fit (template and harmonic functions). The blue dashed line shows the second-order harmonic component, Y_2^{ridge}, and the orange dotted line shows the third-order harmonic component, Y_3^{ridge} (the $n = 2$ and $n = 3$ contributions to the sum in Eq. 1, respectively). The lower panels show the difference between the central data and the peripheral template along with the second and third harmonic functions. The resulting $v_{2,2}$, $v_{3,3}$, and global fit χ^2/NDF values are reported in the legends. In these fits, NDF= 35

By assuming this relation and making specific p_{T} selections on A- and B-particles, the single-particle $v_n(p_{\mathrm{T}}^{\mathrm{A}})$ can be obtained from

$$v_n(p_{\mathrm{T}}^{\mathrm{A}}) = v_{n,n}(p_{\mathrm{T}}^{\mathrm{A}}, p_{\mathrm{T}}^{\mathrm{B}})/\sqrt{v_{n,n}(p_{\mathrm{T}}^{\mathrm{B}}, p_{\mathrm{T}}^{\mathrm{B}})},$$

where $v_{n,n}(p_{\mathrm{T}}^{\mathrm{A}}, p_{\mathrm{T}}^{\mathrm{B}})$ is determined with A- and B-particles having p_{T} in range $p_{\mathrm{T}}^{\mathrm{A}}$ and $p_{\mathrm{T}}^{\mathrm{B}}$, respectively, and $v_{n,n}(p_{\mathrm{T}}^{\mathrm{B}}, p_{\mathrm{T}}^{\mathrm{B}})$ is determined with A- and B-particles both having p_{T} in range $p_{\mathrm{T}}^{\mathrm{B}}$. In this analysis, this range is nominally $p_{\mathrm{T}}^{\mathrm{B}} > 0.4$ GeV, although the dependence of the extracted anisotropy on this choice is explored in Sect. 7.

The relative yield of particle pairs entering the correlation functions is estimated assuming a simple, two-component model of particle production. Particles are assumed to be produced either by hard scattering (HS) processes, such as jet production, or by soft underlying event (UE) processes. With this assumption, the correlation functions are constructed from pairs pulled from a mixture of the two sources. Particle pairs can be formed in the following four A–B combinations: UE–UE, UE–HS, HS–UE, and HS–HS. The event-by-event yields of the UE and HS processes are estimated by classifying the charged particles according to their azimuthal orientation relative to the leading jet or, in the case of MBT events that contain no jets with $p_{\mathrm{T}} > 15$ GeV and $|\eta| < 4.9$, relative to the leading hadron. The following regions are defined relative to this leading vector:

- towards: $(|\phi_{\mathrm{B}} - \phi_{\mathrm{jet}}| < \frac{\pi}{4}) \cup (|\phi_{\mathrm{B}} - \phi_{\mathrm{jet}}| > \frac{3\pi}{4})$
- transverse: $\frac{\pi}{4} < |\phi_{\mathrm{B}} - \phi_{\mathrm{jet}}| < \frac{3\pi}{4}$.

Then, assuming that HS particles are completely contained in the towards region and the UE particles are distributed uniformly in azimuth, the following relations are inferred:

$$N_{\mathrm{UE}} = 2N_{\mathrm{trans}},$$
$$N_{\mathrm{HS}} = N_{\mathrm{toward}} - N_{\mathrm{trans}},$$

where N_{UE} and N_{HS} are the single-particle yields from UE and HS processes, respectively, and N_{trans} and N_{toward} are the particle yields in the transverse and toward regions, respectively. The quantities N_{UE} and N_{HS} are statistically determined from the event averaged N_{trans} and N_{toward} and are, thus, insensitive to event-by-event fluctuations. However, it is not possible to classify individual particles. It should be noted that the assumptions used in this derivation are likely not perfect; for example, the UE is not uniformly distributed in ϕ, event by event, due to the presence of azimuthal anisotropy. The leading object may be more likely to be oriented with the

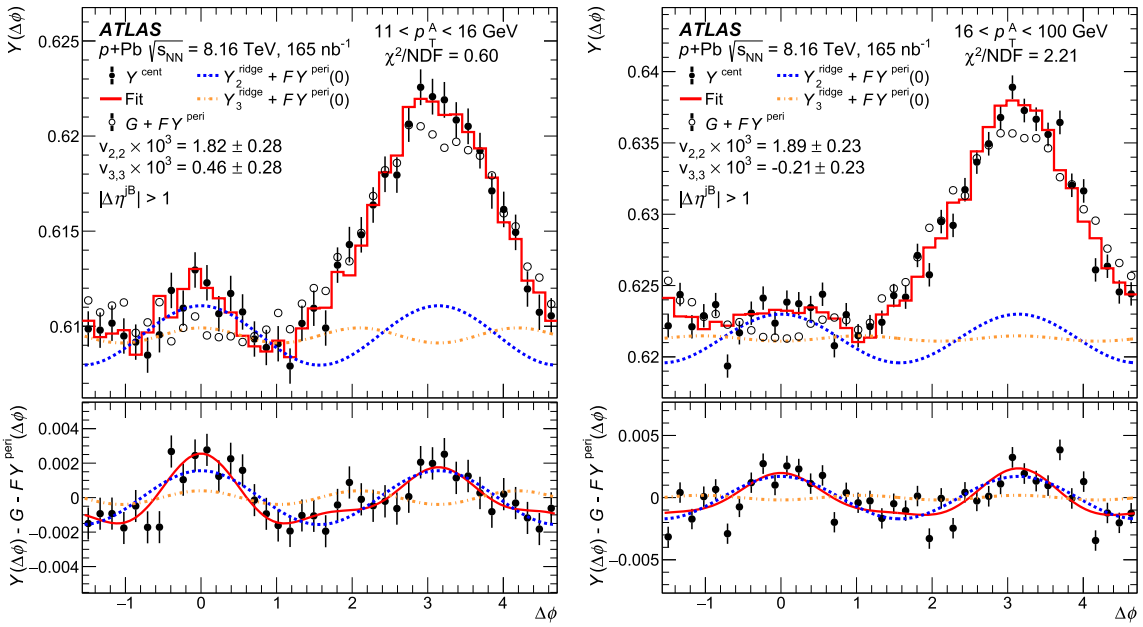

Fig. 2 Template fitting output for events with jet $p_{\mathrm{T}} > 100$ GeV with 60–90% peripheral selection and 0–5% central selection. The left plot is made with $11 < p_{\mathrm{T}}^{\mathrm{A}} < 16$ GeV and the right plot with $16 < p_{\mathrm{T}}^{\mathrm{A}} < 100$ GeV. In the upper panels, the open circles show the scaled and shifted peripheral template with uncertainties omitted, the closed circles show the central data, and the red line shows the fit (template and harmonic functions). The blue dashed line shows the second-order harmonic component, Y_2^{ridge}, and the orange dotted line shows the third-order harmonic component, Y_3^{ridge} (the $n = 2$ and $n = 3$ contributions to the sum in Eq. 1, respectively). The lower panels show the difference between the central data and the peripheral template along with the second and third harmonic functions. The resulting $v_{2,2}$, $v_{3,3}$, and global fit χ^2/NDF values are reported in the legends. In these fits, NDF = 35

anisotropy, in which case the UE yield would be underestimated and the HS yield overestimated. However, the analysis proceeds with the assumptions as given and includes no additional uncertainty for this potential effect.

The $\Delta\eta^{\mathrm{AB}}$ and $\Delta\eta^{\mathrm{jB}}$ rejections produce a geometric correlation between the yields of A- and B-particles and, thus, the number of pairs is not the simple product of the two individual yields. Accounting for the dependencies, the total yield of particle pairs can be expressed in the following way

$$Y_{\mathrm{X-Z}} = \int_{-2.5}^{2.5} \frac{\mathrm{d}N_{\mathrm{X}}^{\mathrm{A}}(\eta^{\mathrm{A}})}{\mathrm{d}\eta^{\mathrm{A}}} \left[\int_{2}^{5} \frac{\mathrm{d}^2 N_{\mathrm{Z}}^{\mathrm{B}}(\eta^{\mathrm{A}}, |\Delta\eta^{\mathrm{AB}}|)}{\mathrm{d}\eta^{\mathrm{A}} \mathrm{d}|\Delta\eta^{\mathrm{AB}}|} \mathrm{d}|\Delta\eta^{\mathrm{AB}}| \right] \mathrm{d}\eta^{\mathrm{A}}, \tag{2}$$

where X–Z could be any pairwise combination of UE and HS. In the case of jet events, the $\Delta\eta^{\mathrm{jB}}$ condition is enforced when filling the η^{A} and $\Delta\eta^{\mathrm{AB}}$ distributions so it's effects are taken into account.

6 Systematic uncertainties

The systematic uncertainties fall into two categories: those associated with both the MBT and jet events and those associated with only the jet events. The uncertainties are determined by assessing the difference between the nominal value of v_2 or v_3 and the value after a given variation. Unless otherwise stated, the uncertainties are defined as asymmetric one-standard-deviation errors. The final uncertainty is the quadrature sum of the uncertainty from each individual source. The relative downward and upward systematic uncertainties from different sources and all sources combined are shown for v_2 in Table 1 and for v_3 in Table 2. The rest of this section focuses primarily on the systematic uncertainties of v_2. While the absolute uncertainties in v_2 and v_3 are of similar magnitude, this represents larger relative uncertainties in the v_3 values since they are generally smaller than the v_2 values at any given p_{T}.

For both the MBT and jet events, the sensitivity to the trigger and tracking efficiency corrections was assessed by removing each. This variation ('Track/trig Eff.' in Table 1) yields a 0–2% (2–4%) difference for MBT (jet) events, depending on track p_{T}, and is subdominant. In the construction of the correlation functions, the uncertainty in the mixed-event correction was again found by removing it from the analysis. This variation results in an uncertainty that vanishes at low p_{T} but grows to 20% (10%) at high p_{T} for MBT (jet) events, but remains subdominant to statistical uncertainties over the whole p_{T} range. Regarding the template fitting procedure, the centrality range for the peripheral reference

Table 1 Systematic uncertainty summary for anisotropy coefficients v_2. The values are approximate, as they represent the average variation in each p_T range, and are reported relative to v_2. Negative and positive values indicate downward and upward uncertainties respectively. Commas separate the downward and upward uncertainty where applicable

Source	$p_T < 2$ GeV		$p_T = 2$–10 GeV		$p_T > 10$ GeV	
	MBT	Jet	MBT	Jet	MBT	Jet
Track/trig Eff.	$< +1\%$	$+2\%$	$< +1\%$	$+4\%$	-2%	$+2\%$
Mixed event	$< +1\%$	$< +1\%$	-4%	$+4\%$	$+20\%$	$+10\%$
Peri. reference	$-1, +2\%$	$-2, +2\%$	$-2, +10\%$	$-10, +18\%$	$-10, +10\%$	$-2, +10\%$
Trig jet p_T	–	$< +1\%$	–	$-6, +6\%$	–	$-10, +10\%$
Reject jet p_T	–	$-2, +2\%$	–	$-5, +5\%$	–	$-10, +10\%$
Reject jet mult.	–	$< +1\%$	–	-5%	–	-5%
Disabled HEC sector	–	$< +1\%$	–	$+10\%$	–	$+20\%$
Jet-UE bias	–	-5%	–	-15%	–	-25%
Total	$-1, +2\%$	$-5, +4\%$	$-5, +10\%$	$-20, +20\%$	$-10, +25\%$	$-30, +25\%$

Table 2 Systematic uncertainty summary for anisotropy coefficients v_3. The values are approximate, as they represent the average variation in each p_T range, and are reported relative to v_3. Negative and positive values indicate downward and upward uncertainties respectively. Commas separate the downward and upward uncertainty where applicable

Source	$p_T < 2$ GeV		$p_T = 2$–10 GeV		$p_T > 10$ GeV	
	MBT	Jet	MBT	Jet	MBT	Jet
Track/trig Eff.	$+1\%$	$+4\%$	$< +6\%$	-7%	-5%	-7%
Mixed event	$< +1\%$	-4%	-20%	$+6\%$	-200%	$+20\%$
Peri. reference	$-2, +2\%$	$-7, +10\%$	$-8, +8\%$	$-20, +10\%$	$-150, +100\%$	$-30, +30\%$
Trig jet p_T	–	$< +1\%$	–	$-10, +10\%$	–	$-40, +40\%$
Reject jet p_T	–	$-2, +2\%$	–	$-15, +15\%$	–	$-15, +15\%$
Reject jet mult.	–	$< +1\%$	–	$+5\%$	–	$+20\%$
Disabled HEC sector	–	-2%	–	-5%	–	-10%
Total	$-2, +2\%$	$-10, +10\%$	$-20, +10\%$	$-30, +20\%$	$-250, +100\%$	$-50, +50\%$

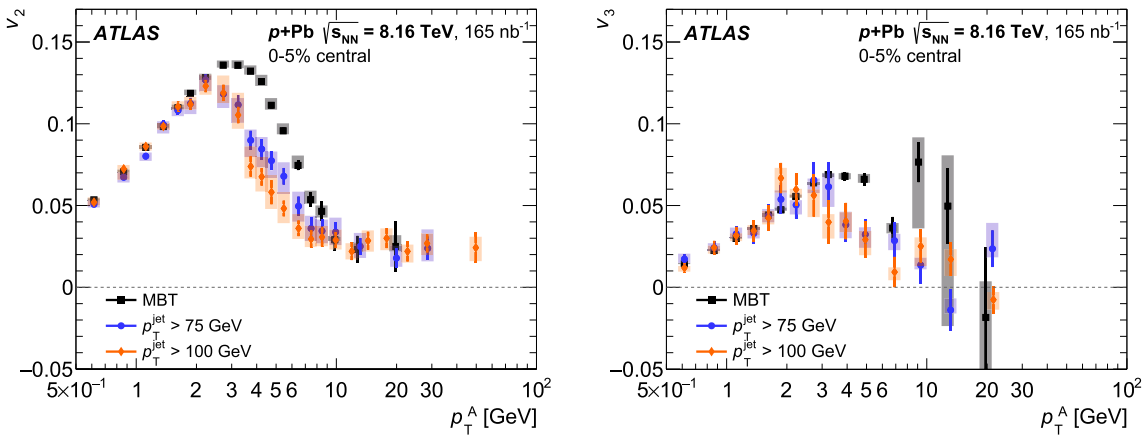

Fig. 3 Distribution of v_2 (left) and v_3 (right) plotted as a function of the A-particle p_T. Values from MBT events are plotted as black squares, and those from events with jet $p_T > 75$ GeV and events with jet $p_T > 100$ GeV are plotted as blue circles and orange diamonds respectively. Statistical uncertainties are shown as narrow vertical lines on each point, and systematic uncertainties are presented as coloured boxes behind the points

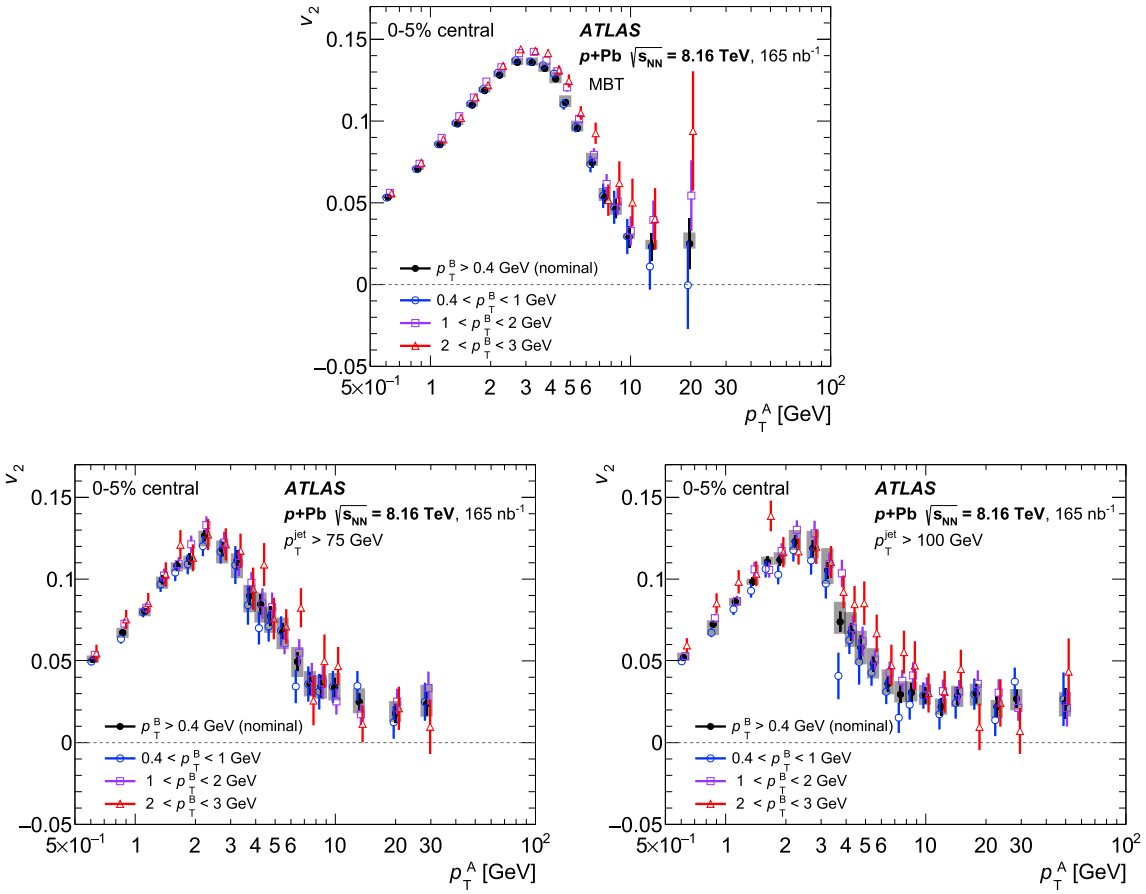

Fig. 4 Measured v_2 values plotted as a function of the A-particle p_{T} for MBT events (top), events with jet $p_{\mathrm{T}} > 75$ GeV (bottom left), and events with jet $p_{\mathrm{T}} > 100$ GeV (bottom right). The nominal values (closed black circles) are overlaid with points generated by making different B-particle p_{T} selections: $0.4 < p_{\mathrm{T}}^{\mathrm{B}} < 1$ GeV (blue open circles), $1 < p_{\mathrm{T}}^{\mathrm{B}} < 2$ GeV (open violet squares), and $2 < p_{\mathrm{T}}^{\mathrm{B}} < 3$ GeV (open red triangles). The points with different B-particle p_{T} selections are offset slightly from the nominal horizontal-axis positions to make the uncertainties visible. For clarity, systematic uncertainties are omitted from the three sets of restricted B-particle p_{T} ranges; they are, however, consistent with those from the inclusive results and are highly correlated between the selections

selection was varied from the nominal 60–90% to 50–70% and 70–90%. This variation ('Peri. reference') results in an uncertainty of about 2% at low p_{T} and increasing to about 10% or 18% in the mid p_{T} range between 2 and 10 GeV depending on the event trigger. This last uncertainty is dominant in this category for most of the p_{T} range probed in the measurement. At high p_{T}, the sensitivity of the measurements in MBT events to the mixed event correction and reference selection is significantly higher than in jet events; this is particularly noticeable for the v_3 values, where the relative uncertainties in the MBT events for $p_{\mathrm{T}} > 10$ GeV are 5–10 times larger than in the jet-triggered events.

The following set of uncertainties is associated with jet events only. To assess the sensitivity to the uncertainty in the jet energy scale and the impact of imperfect trigger efficiency, the jet p_{T} thresholds used to select events were varied from 75 GeV and 100 GeV to 80 GeV and 105 GeV, respectively. This variation ('Trig jet p_{T}') results in a symmetric uncertainty that is smaller than 1% at low particle p_{T} and that increases to about 10% with increasing p_{T}. It is subdominant to other sources in this category. The jets used in the B-particle jet rejection were varied to include only jets with p_{T} greater than 20 GeV instead of the nominal 15 GeV ('Reject jet p_{T}'). The 2% and 10% differences at low and high p_{T} are incorporated as a symmetric uncertainty that is subdominant to other sources in this category. The $\Delta\eta^{\mathrm{jB}}$ rejection allows jets to be composed of only a single particle that may originate in the tail of the UE particle p_{T} spectrum. Thus, the jets used in this rejection were varied to require at least three tracks in a $\Delta R = 0.4$ cone around the jet axis ('Reject jet mult.'). The uncertainty associated with this variation is about 5% and subdominant to the others in this category. An additional uncertainty is used to cover the impact of a sector of the hadronic endcap calorimeter (HEC) being disabled for the running period. The disabled sector was in the range $1.5 < \eta < 3.2$ and $-\pi < \phi < -\pi/2$. This uncer-

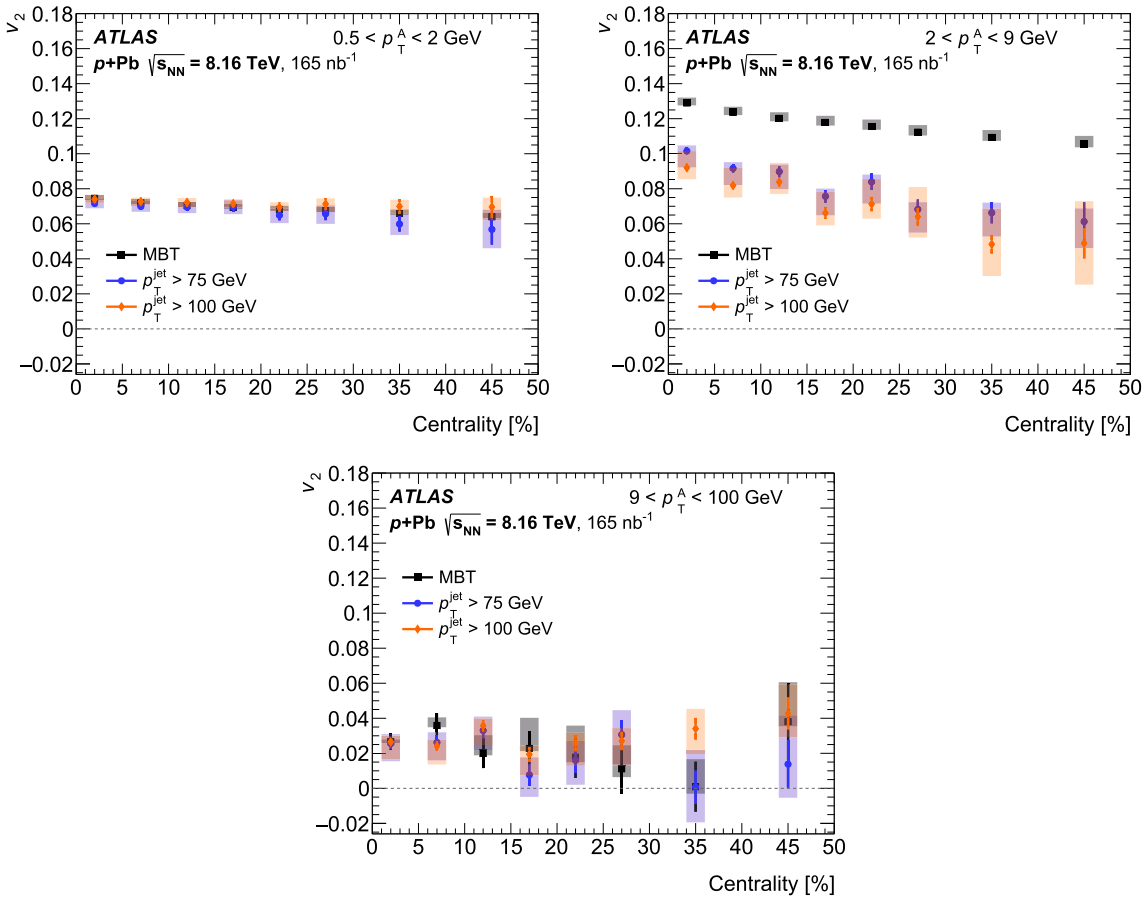

Fig. 5 Distribution of v_2 plotted as a function of centrality for MBT events (black squares), events with jet $p_{\mathrm{T}} > 75$ GeV (blue circles), and events with jet $p_{\mathrm{T}} > 100$ GeV (orange diamonds). The results are obtained in three different selections of the A-particle p_{T}: $0.5 < p_{\mathrm{T}} < 2$ GeV (top left), $2 < p_{\mathrm{T}} < 9$ GeV (top right), and $9 < p_{\mathrm{T}} < 100$ GeV (bottom). Statistical uncertainties are shown as narrow vertical lines on each point, and systematic uncertainties are presented as coloured boxes behind the points

tainty ('Disabled HEC sector') was assessed by requiring all B-particles to be outside the pseudorapidity region of the disabled HEC. The difference was found to be less than 1% at low p_{T} and about 20% at high p_{T}, where it is the dominant positive uncertainty. Finally, an uncertainty is assigned to account for the potential of the UE to bias the event selection. The azimuthal modulation of the UE increases the reconstructed p_{T} of jets aligned with the flow orientation, and, thus, the event-wise jet-p_{T} threshold will bias the events to have more jets correlated with the flow plane. The impact of this effect on the measured results was assessed in simulation by mixing jet events with a realistic UE containing azimuthal anisotropy. The resulting uncertainty only affects v_2, is the dominant negative uncertainty for track p_{T} greater than 3 GeV, and is about 30% (20%) for jet-triggered events with jet $p_{\mathrm{T}} > 75$ GeV (100 GeV). The effect is larger for lower-p_{T} jets because the UE energy contribution is independent of jet energy. For a power-law spectrum, a given threshold change has a greater fractional effect on the yield for smaller values of the threshold.

In summary, the uncertainty in v_2 from the peripheral reference selection was found to be dominant for p_{T} less than 10 GeV for MBT events, above which, the mixed event correction uncertainty is dominant, and between 2 and 5 GeV for jet events. The uncertainties associated with the jet selection were found to be dominant for $p_{\mathrm{T}} \gtrsim 10$ GeV in jet events. The total uncertainty in MBT events ranges from $(-1\%, +2\%)$ at low p_{T} to about $(-10\%, +25\%)$ at high p_{T}. For jet events, the total uncertainty ranges from about $(-5\%, +4\%)$ at low p_{T} to about $(-35\%, +50\%)$ and $(-30\%, +25\%)$ at high p_{T} for events with jet $p_{\mathrm{T}} > 75$ GeV and jet $p_{\mathrm{T}} > 100$ GeV respectively.

The uncertainties associated with the measurement of particle pair yields are generated from some of the variations discussed above, namely the track and trigger efficiency variation, the trigger jet p_{T} threshold variation, and each B-particle jet rejection variation. An additional variation was made to

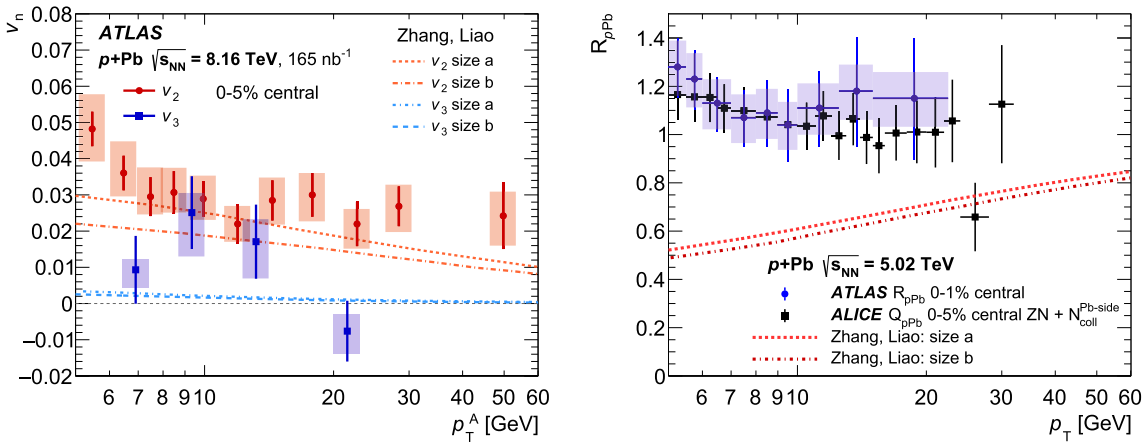

Fig. 6 Coefficients v_2 and v_3 (left panel) and $R_{p\mathrm{Pb}}$ (right panel) plotted as a function of particle p_T for p+Pb collisions. The left panel is for central 0–5% events from the jet $p_\mathrm{T} > 100$ GeV event sample. Statistical uncertainties are shown as narrow vertical lines on each point, and systematic uncertainties are presented as coloured boxes behind the points. The left panel has two sets of curves showing theoretical predictions from a jet quenching framework with two different initial geometries in 0–4% central collisions [14]; the upper two (red/orange) are v_2 for 'size a' (dotted) and 'size b' (dash-dotted) configurations, and the lower two (blue) are v_3 where the 'size a' (dash-dotted) and 'size b' (dashed) curves are nearly indistinguishable from each other. The right panel shows $R_{p\mathrm{Pb}}$ data from ATLAS [57] and $Q_{p\mathrm{Pb}}$ data from ALICE [41]. Theoretical calculations (red/orange lines) from Ref. [14] are also shown in this panel; the dotted line gives the results of the 'size a' configuration and the dash-dotted line gives the results of the 'size b' configuration

test the assumption that the toward region contains all HS particles. The two transverse region sides were tagged as having the minimum and maximum number of tracks out of the two. The pair yields were, then, calculated using the minimum and maximum sides only, as separate variations. This variation produces the dominant uncertainty in the relative pair yields, defined in Eq. (2), for all particle combinations at all p_T.

7 Results

Figure 3 shows the extracted second- (v_2) and third-order (v_3) anisotropy coefficients for the MBT events compared to those from both selections of jet events plotted as a function of A-particle p_T in the range $0.5 < p_\mathrm{T} < 100$ GeV. Each set of values is from events with the same 0–5% centrality selection. Points are located on the horizontal axis at the mean p_T of tracks within any given bin. The v_2 and v_3 coefficients increase as a function of p_T in the low p_T region ($p_\mathrm{T} <$ 2–3 GeV), then decrease (2–3 $< p_\mathrm{T} <$ 9 GeV), and finally plateau for high p_T ($p_\mathrm{T} >$ 9 GeV). The v_2 coefficients are consistent with being independent of p_T for $p_\mathrm{T} > 9$ GeV, while the larger uncertainties in the values of v_3 preclude any strong conclusion.

The v_2 results show agreement within uncertainties between the MBT and jet events for the low p_T ($p_\mathrm{T} \lesssim 2$ GeV) and high p_T ($p_\mathrm{T} \gtrsim 9$ GeV) regions. For the intermediate p_T region, the MBT events yield a higher v_2 value than jet events, although the trends are qualitatively similar. Similarly to v_2, the v_3 results show agreement between the MBT and jet events for $p_\mathrm{T} < 2$ GeV, and higher values from MBT events for $p_\mathrm{T} > 2$ GeV.

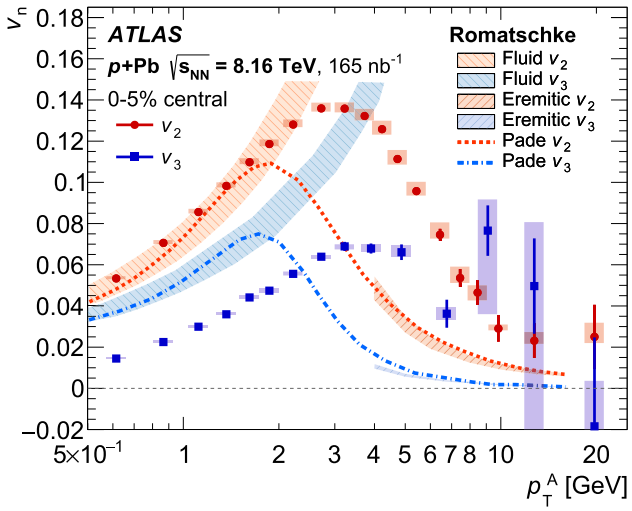

Fig. 7 Coefficients v_2 and v_3 plotted as a function of p_T for central 0–5% p+Pb collisions from the MBT event sample. Theoretical calculations relevant to the low-p_T regime from hydrodynamics and to the high-p_T regime from an 'eremitic' framework from Romatschke [26] are also shown. The lines are Padé-type fits connecting the two regimes, where the red dotted line is for v_2 and the blue dash-dotted line is for v_3. Statistical uncertainties are shown as narrow vertical lines on each point, and systematic uncertainties are presented as coloured boxes behind the points

As mentioned in Sect. 5, if the measured anisotropy originates from a global momentum field, the v_2 and v_3 values,

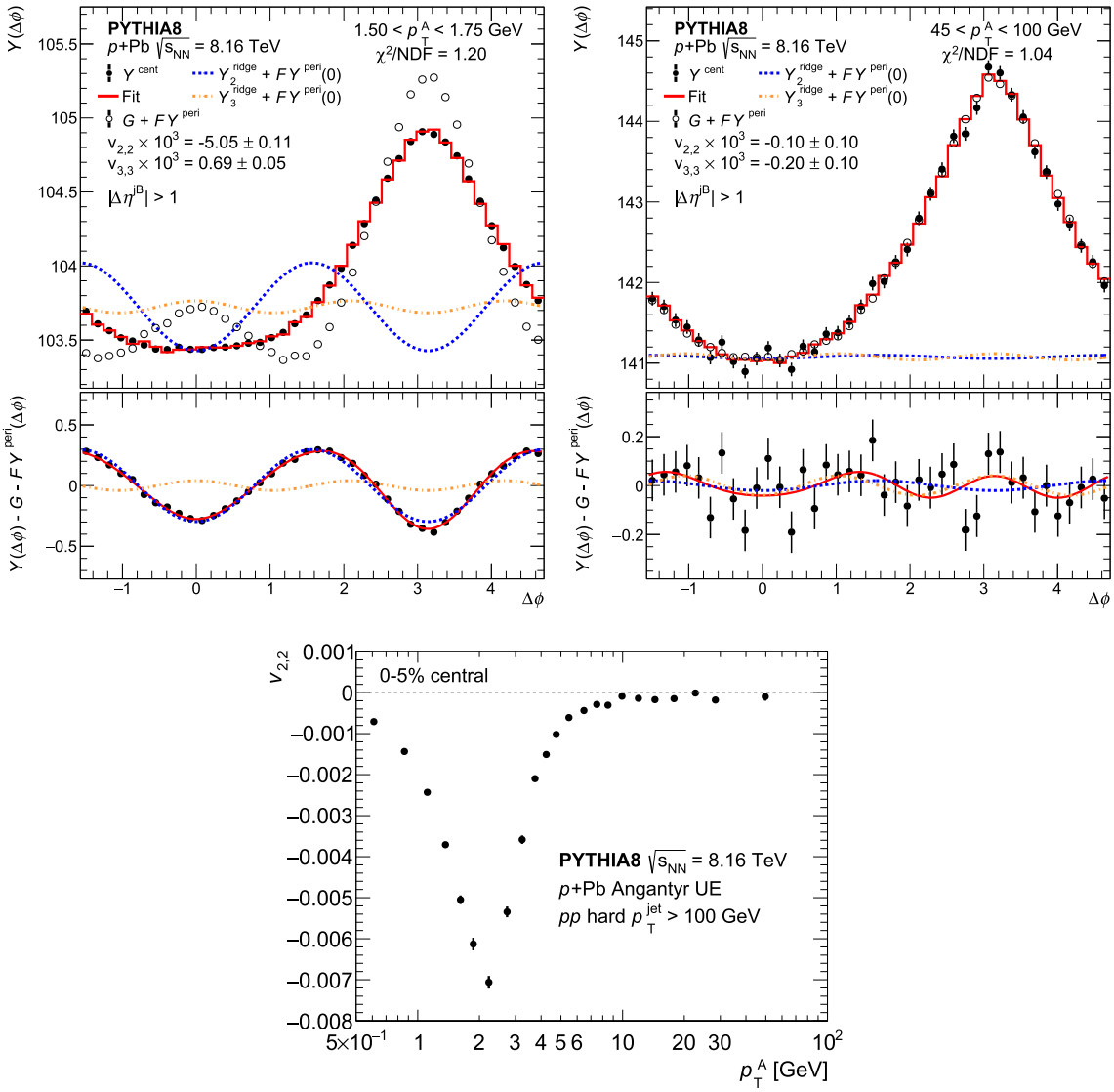

Fig. 8 Predictions of azimuthal anisotropy from PYTHIA 8 using the same two-particle formalism used for the data results. The events combine minimum-bias p+Pb underlying events generated in the Angantyr framework with hard pp events that require the presence of a jet with $p_{\mathrm{T}} > 100$ GeV. The two top plots show example correlation functions, with template fits, from a low particle-p_{T} selection (top left) and a high particle-p_{T} selection (top right). In the upper panels of the two top plots, the open circles show the scaled and shifted peripheral template with uncertainties omitted, the closed circles show the central data, and the red histogram shows the fit (template and harmonic functions). The blue dashed line shows the second-order harmonic component, Y_2^{ridge}, and the orange dashed line shows the third-order harmonic component, Y_3^{ridge} (the $n = 2$ and $n = 3$ contributions to the sum in Eq. 1, respectively). The lower panels show the difference between the central data and the peripheral template along with the second and third harmonic functions. The resulting $v_{2,2}$, $v_{3,3}$, and global fit χ^2/NDF values are reported in the legends, where NDF $= 35$. The bottom plot shows the extracted $v_{2,2}$ values as a function of A-particle p_{T}

extracted for a given $p_{\mathrm{T}}^{\mathrm{A}}$ range, will be independent of B-particle selection. This assumption of factorisation is explicitly tested by carrying out the analysis for different selections of $p_{\mathrm{T}}^{\mathrm{B}}$. Figure 4 shows the v_2 values, from each event trigger, for the nominal results using $p_{\mathrm{T}}^{\mathrm{B}} > 0.4$ GeV overlaid with results using $0.4 < p_{\mathrm{T}}^{\mathrm{B}} < 1$ GeV, $1 < p_{\mathrm{T}}^{\mathrm{B}} < 2$ GeV, and $2 < p_{\mathrm{T}}^{\mathrm{B}} < 3$ GeV. The test shows factorisation breaking at the level of 5% for $p_{\mathrm{T}}^{\mathrm{A}} < 5$ GeV in MBT events. However, at higher $p_{\mathrm{T}}^{\mathrm{A}}$, the differences grow with $p_{\mathrm{T}}^{\mathrm{A}}$ to be 10–100% from the nominal values. For jet events, factorisation holds within about 10–20% for all values of $p_{\mathrm{T}}^{\mathrm{A}}$, except for $4 < p_{\mathrm{T}}^{\mathrm{A}} < 9$ GeV in $p_{\mathrm{T}}^{\mathrm{jet}} > 100$ GeV events, where it is within about 30–40%. Although the large uncertainties prevent strong conclusions from being drawn, there is a hint of a difference in behaviour at high $p_{\mathrm{T}}^{\mathrm{A}}$ where the factorisation breaking is greater for MBT events than for jet events. This result could be due to the B-particle jet rejection scheme used for the jet events. Correlations resulting from hard-process,

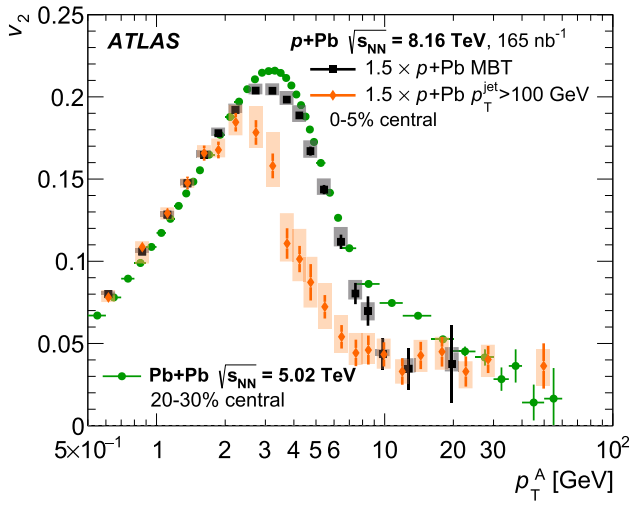

Fig. 9 Scaled p+Pb v_2 values plotted as a function of the A-particle p_{T} overlaid with v_2 from 20–30% central Pb+Pb data at $\sqrt{s_{\mathrm{NN}}}$ = 5.02 TeV [62]. Results from MBT and jet $p_{\mathrm{T}} > 100$ GeV p+Pb events are plotted as black squares and orange diamonds, respectively, and those from Pb+Pb are plotted as green circles. Statistical uncertainties are shown as narrow vertical lines on each point, and systematic uncertainties are presented as coloured boxes behind the points

e.g. from back-to-back jets, specifically violate the factorisation assumption, and the B-particle jet rejection dramatically limits the contribution from these processes from entering the correlation functions in jet events. However, the correlations from MBT events have no such rejection, and could, therefore, be more susceptible to hard-process correlations at high $p_{\mathrm{T}}^{\mathrm{A}}$.

Figure 5 shows v_2 plotted as a function of centrality for MBT events and both classes of jet events. The results are divided into three regions in A-particle p_{T}: $0.5 < p_{\mathrm{T}} < 2$ GeV, $2 < p_{\mathrm{T}} < 9$ GeV, and $9 < p_{\mathrm{T}} < 100$ GeV. The v_2 results show agreement, within uncertainties, between the MBT and jet events for p_{T} selections $0.5 < p_{\mathrm{T}} < 2$ GeV and $p_{\mathrm{T}} > 9$ GeV for all centralities and are found to be nearly independent of centrality. For $2 < p_{\mathrm{T}} < 9$ GeV, the MBT events give a higher v_2 value than the jet events, and all three sets show a trend to lower values of v_2 as the collisions become more peripheral.

Focusing on the overall p_{T} dependence of the anisotropies, Fig. 6 (left panel) shows v_2 and v_3 coefficients from events with jet $p_{\mathrm{T}} > 100$ GeV compared with theoretical calculations from Ref. [14]. This theoretical calculation, within the jet quenching paradigm, invokes a stronger parton coupling to the QGP near the transition temperature, which helps to reduce the tension in simultaneously matching the nucleus–nucleus high-p_{T} hadron spectrum suppression and the azimuthal anisotropy v_2. The calculation tests two different initial p+Pb geometries referred to as 'size a' and 'size b', where the latter has a smaller initial QGP volume. The predictions are slightly lower than the data for both v_2 and v_3, and the 'size a' curve is within two standard deviations of all points. However, in the right panel of Fig. 6, the same calculation predicts a substantial suppression of high-p_{T} hadrons, as expressed by the quantity $R_{p\mathrm{Pb}} = \mathrm{d}^2N_{p\mathrm{Pb}}/\mathrm{d}p_{\mathrm{T}}\mathrm{d}y/(T_{p\mathrm{Pb}} \times \mathrm{d}^2\sigma_{pp}/\mathrm{d}p_{\mathrm{T}}\mathrm{d}y)$ where $T_{p\mathrm{Pb}}$ represents the nuclear thickness of the Pb nucleus, as determined via a Monte Carlo Glauber calculation [56]. Shown in comparison are published experimental results from ATLAS and ALICE for $R_{p\mathrm{Pb}}$ in central events that are consistent with no nuclear suppression, i.e. $R_{p\mathrm{Pb}} = 1$ [41,57]. The ALICE experiment uses the notation $Q_{p\mathrm{Pb}}$ for the same quantity to describe a bias that may exist due to the centrality categorisation. There are uncertainties in the experimental measurements related to the centrality or multiplicity selection in p+Pb collisions, particularly in determining the nuclear thickness value $T_{p\mathrm{Pb}}$. However, there is no indication of the large $R_{p\mathrm{Pb}}$ suppression predicted by the jet quenching calculation. Thus, the jet quenching calculation is disfavoured as it cannot simultaneously describe the non-zero high-p_{T} azimuthal anisotropy and the lack of yield suppression.

Figure 7 shows the MBT v_2 and v_3 coefficients compared with theoretical calculations from Ref. [26]. The calculations are derived from two opposite limits of kinetic theory. The low momentum bands represent zeroth-order hydrodynamic calculations for high-multiplicity p+Pb events that give quantitative agreement with v_2 up to $p_{\mathrm{T}} = 2$ GeV while predicting values of v_3 that are too high. Above some high p_{T} threshold, hadrons are expected to result, not from hydrodynamics, but instead from jets where the resulting partons have the opposite limit than in hydrodynamics, i.e. a large mean free path. To model this region, a non-hydrodynamic 'eremitic' expansion calculation (see Ref. [26] for the detailed calculation), shown as the bands at high p_{T}, indicates slowly declining v_2 and v_3 coefficients. The dashed lines are a simple Padé-type fit connecting the two regimes [26]. The trends are qualitatively similar to those in the data, although there is not quantitative agreement. In particular, the calculation predicts values of v_2 and v_3 substantially below the experimental results for $p_{\mathrm{T}} = 4$–15 GeV. It should be noted that calculations presented in Ref. [26] are performed, consistently between the hydrodynamic and eremitic components, only for massless partons and with an ideal equation of state. Thus, one does not expect quantitative agreement and is looking for rather qualitative trends. More sophisticated treatments in the hydrodynamic regime result in better quantitative agreement with the anisotropy coefficients at low p_{T} [58,59]. It is worth highlighting that traditional parton energy-loss calculations connect the high-p_{T} v_2 with a suppression in the overall yield of high-p_{T} particles. The same is true with this eremitic calculation, and thus, it should also be in contradistinction to p+Pb high-p_{T} experimental data indicating almost no suppression, i.e. jet quenching.

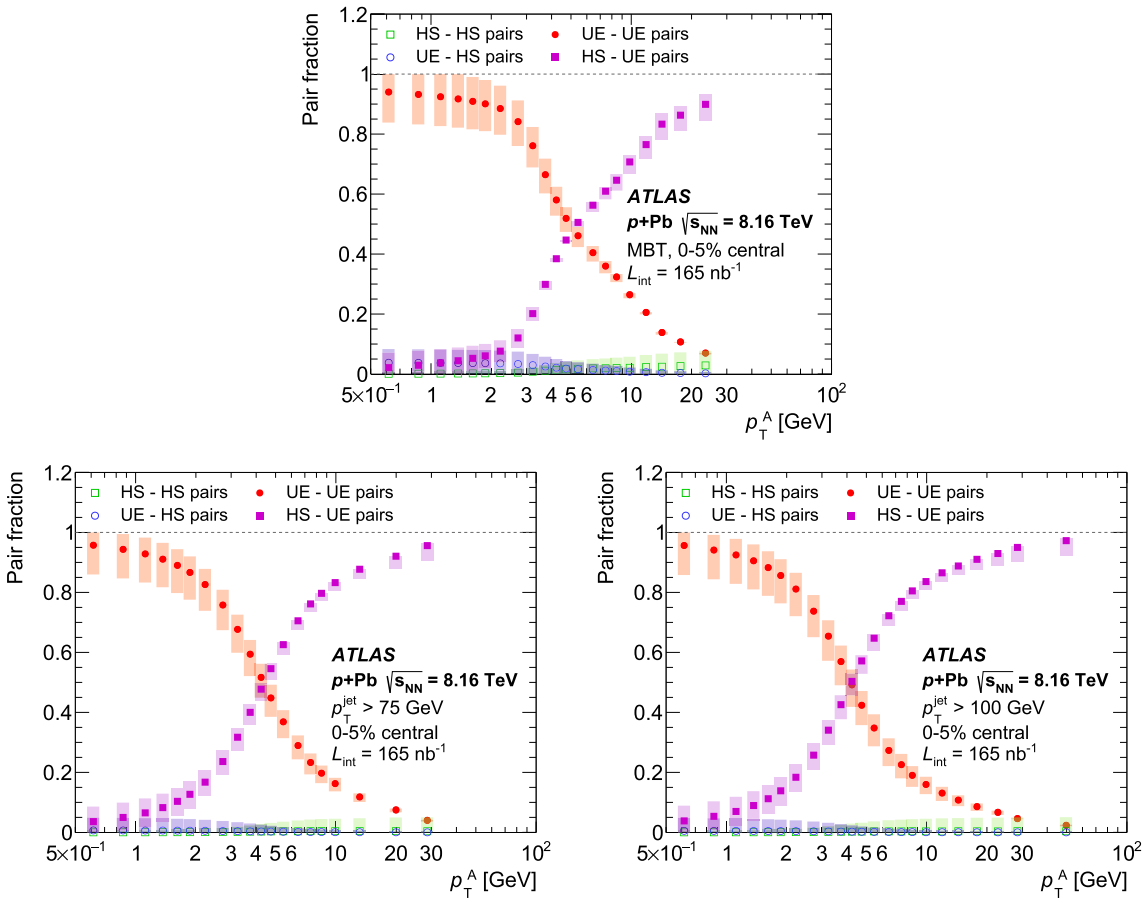

Fig. 10 Particle pair yield composition fractions for MBT events (top), events with jet $p_{\mathrm{T}} > 75$ GeV (bottom left), and events with jet $p_{\mathrm{T}} > 100$ GeV (bottom right) plotted as a function of the A-particle p_{T}. Green and blue open circles represent HS–HS and UE–HS pairs, respectively, and red and violet closed circles represent UE–UE and HS–UE pairs, respectively. Statistical uncertainties are shown as narrow vertical lines on each point, and systematic uncertainties are presented as coloured boxes behind the points

Another possible source of the high-p_{T} anisotropies could lie in an initial-state effect, potentially encoded in a model such as PYTHIA 8. Shown in Fig. 8 is a PYTHIA 8 calculation with hard[2] pp events overlaid on minimum-bias p+Pb events generated in the default Angantyr framework [60]. It is emphasised that this version of PYTHIA does not include the recently developed string–string, or so-called string shoving, implementation [61]. The generator-level charged particles are then processed with the entire analysis procedure, including the non-flow template fit. The result is a negative $v_{2,2}$ for all momenta, in contradistinction to the experimental data. Further investigation reveals that PYTHIA 8 run in 'hard' scattering mode has correlations with large pseudorapidity separation between particle pairs as a result of the specific implementation of initial-state radiation. This correlation is reduced in high-multiplicity events because of the large number of uncorrelated UE particles, and thus results in a negative $v_{2,2}$ after subtracting the non-flow contribution.

Figure 9 shows the published Pb+Pb results for v_2 as a function of p_{T} in the 20–30% centrality selection [62] compared to the v_2 from both the MBT p+Pb data and p+Pb containing a jet with $p_{\mathrm{T}} > 100$ GeV. This Pb+Pb centrality range is selected because the spatial elliptic eccentricity is approximately the same as in 0–5% centrality p+Pb collisions [63], despite having a much larger total particle multiplicity. The overall trends for Pb+Pb v_2 as a function of p_{T} are qualitatively similar to those presented here for p+Pb from MBT events and the jet events with jet $p_{\mathrm{T}} > 100$ GeV. Both sets of the p+Pb values are scaled by a single multiplicative factor (1.5) to match the Pb+Pb rise at low p_{T}. After scaling, the MBT p+Pb results quantitatively agree with those from the Pb+Pb system for $0.5 < p_{\mathrm{T}} < 8$ GeV, except for a slight difference in the peak value near $p_{\mathrm{T}} \approx 3$ GeV. For p_{T} above about 8 GeV, the Pb+Pb results indicate a slow decline of v_2 values with increasing p_{T}, while the p+Pb results exhibit

[2] The term 'hard' refers to PYTHIA 8 run with the following settings: `HardQCD:all=on`, `PartonLevel:MPI=off`, and containing a jet with $p_{\mathrm{T}} > 100$ GeV.

more of a plateau. Strikingly, the overall behaviour of the v_2 values are quite similar.

As described above, the physics interpretations of the Pb+Pb elliptic anisotropies are hydrodynamic flow at low p_T, differential jet quenching at high p_T, and a transition between the two in the intermediate region of approximately $2 < p_T < 10$ GeV. Since these effects all relate to the initial QGP geometric inhomogeneities, a common shape with a single scaling factor for p+Pb could indicate a common physics interpretation. This scaling factor of 1.5, as empirically determined, may be the result of slightly different initial spatial deformations, or from the much larger Pb+Pb overall multiplicity, which enables a stronger translation of spatial deformations into momentum space. For the high p_T region, this presents a conundrum in that it is difficult for differential jet quenching to cause the v_2 anisotropy in p+Pb collisions when there is no evidence for jet quenching overall. These measurements showing non-zero high p_T v_2 in p+Pb collisions in the absence the jet quenching observed in Pb+Pb collisions suggest there might be additional contributions to v_2 at high p_T in Pb+Pb collisions.

Returning to the issue of the difference in the intermediate p_T region between the p+Pb MBT and jet event results, the source of hadrons in this region should be considered. As detailed previously, in a highly simplified picture one can classify hadrons as originating from hard scatterings (HS) or from the underlying event (UE). Thus, pairs of particles of A and B types can come from the combinations HS–HS, HS–UE, UE–HS, and UE–UE. Figure 10 presents the measured pair fractions for both MBT and jet, 0–5% central events plotted as a function of the A-particle p_T. UE–UE pairs dominate the correlation functions at low p_T in each case, and HS–UE combinations dominate at high p_T. Combinations with HS B-particles are sub-dominant, because there are fewer jet particles than UE particles in central events; for the jet selected events, these combinations are further suppressed by the B-particle jet rejection condition. Figure 11 shows the dominant contributions from the MBT and jet events overlaid. Although the same qualitative behaviour is found in each case, the point at which the HS–UE pairs become dominant over the other combinations is at a lower p_T for jet events than for MBT events.

This behaviour can also be seen in Fig. 12, in which the pair fractions are plotted as a function of centrality, and again, the values for MBT and jet events are overlaid. The centrality-dependent results are plotted for low, medium, and high A-particle p_T ranges in the same way as in Fig. 5. At low p_T, pair fractions from MBT and jet events agree, and in the mid-p_T transition region, MBT events have a larger UE–UE contribution and smaller HS–UE contribution compared to jet events. At high p_T, central events show a difference between UE–UE and HS–UE that is reduced in more-peripheral events and absent for more peripheral than 25% centrality. The overall

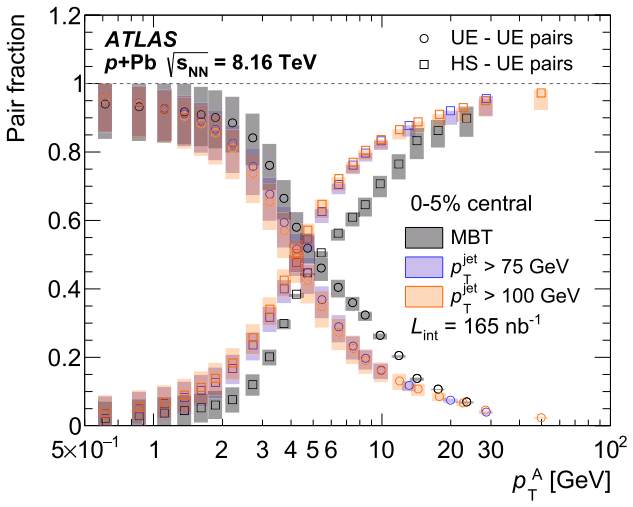

Fig. 11 Underlying event–underlying event (UE–UE) (open circles) and hard scatter–underlying event (HS–UE) (open squares) particle-pair yield composition fractions for MBT events (black), events with jet $p_T > 75$ GeV (blue), and events with jet $p_T > 100$ GeV (orange) plotted as a function of the A-particle p_T. Statistical uncertainties are shown as narrow vertical lines on each point, and systematic uncertainties are presented as coloured boxes behind the points

trend of the pair fractions with centrality is quite similar to that of v_2 shown in Fig. 5; little centrality dependence for low and high p_T, and significant centrality dependence in addition to MBT–jet event ordering in the mid-p_T transition region.

Thus, a potential explanation for the lower v_2 and v_3 in the intermediate p_T region is simply that, in that region, the HS particles have lower anisotropy coefficients than UE particles, and MBT events have a larger fraction of UE–UE pairs than jet-triggered events. In the low and high p_T regions, the same types of pairs dominate in both the MBT and jet-triggered events, namely UE–UE and HS–UE respectively, and hence the anisotropy coefficients agree between the event samples. If this explanation is correct, it also aids in understanding Fig. 9 in which there is a significant difference between the p+Pb jet event v_2 and the Pb+Pb v_2 in the intermediate p_T region, because the relative pair fractions are potentially significantly different.

This particle mixing picture is attractive in that it naturally explains the general shape of the $v_2(p_T)$ and $v_3(p_T)$ distributions as well as the ordering of the different event samples. However, it is noted that the correspondence between the differences in the flow coefficients and pair fractions is not quantitative; the differences in the flow coefficients are fractionally much larger than the differences in the pair fractions. Thus, there are either additional sources of correlation or our assumptions are violated in some way (e.g. the two assumed HS and UE sources are too simplistic or the measured pair fractions do not accurately represent the sources, as is discussed in Sect. 5). That said, for particle $p_T > 20$ GeV, where

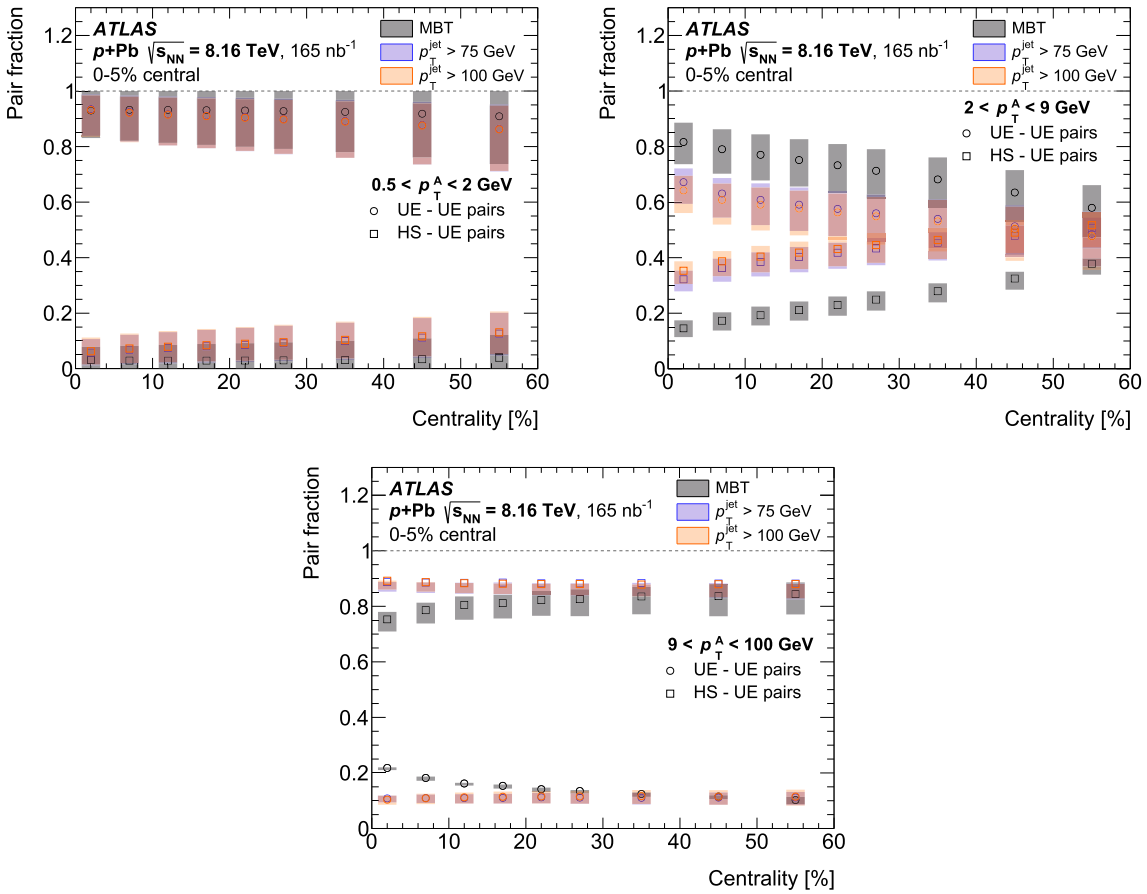

Fig. 12 Underlying event–underlying event (UE–UE) (open circles) and hard scatter–underlying event (HS–UE) (open squares) particle-pair yield composition fractions for MBT events (black), events with jet $p_{\mathrm{T}} > 75$ GeV (blue), and events with jet $p_{\mathrm{T}} > 100$ GeV (orange) plotted as a function of event centrality. The results are obtained in three different selections of the A-particle p_{T}: $0.5 < p_{\mathrm{T}} < 2$ GeV (top left), $2 < p_{\mathrm{T}} < 9$ GeV (top right), and $9 < p_{\mathrm{T}} < 100$ GeV (bottom). Statistical uncertainties are shown as narrow vertical lines on each point, and systematic uncertainties are presented as coloured boxes behind the points

particle production in any model is thought to arise mainly from jet fragmentation, the non-zero v_2 demonstrates that a positive correlation exists between hard (high p_{T}) and soft (low p_{T}) particles, irrespective of the pair fractions.

8 Conclusion

This paper presents Fourier coefficients of the azimuthal distribution of unidentified charged particles from 165 nb^{-1} of $\sqrt{s_{\mathrm{NN}}} = 8.16$ TeV p+Pb collisions at the LHC and measured with the ATLAS detector. Results are presented separately for minimum-bias and jet events, with jet p_{T} thresholds of 75 and 100 GeV, as a function of particle p_{T} and centrality. The results are extracted using two-particle azimuthal correlations combined with a non-flow template fit procedure. The charged particle p_{T} dependence of v_2 and v_3 is found assuming the factorisation of $v_{n,n}$. The v_2 results are presented for charged-particle transverse momentum $p_{\mathrm{T}} = 0.5$–20 GeV for minimum-bias events and $p_{\mathrm{T}} = 0.5$–50 GeV for jet-triggered events, and the v_3 results are for $p_{\mathrm{T}} = 0.5$–20 GeV in both cases.

For charged particles with p_{T} between 0.5 and 2 GeV, the v_n results from each event selection are quantitatively consistent with each other, rising steadily with p_{T}, and the v_2 coefficients are roughly independent of centrality. The v_2 values at 0–5% centrality agree with those predicted by hydrodynamic calculations.

Between charged particle p_{T} of 2 and 9 GeV, the v_n values drop in each case, but are ordered with minimum-bias events yielding the highest v_n values and the jet events with jet $p_{\mathrm{T}} > 100$ GeV the lowest. Charged particles in this p_{T} range exhibit a significant centrality-dependent v_2, monotonically decreasing from central to peripheral events. This behaviour can be qualitatively explained within a simplified two-component model of particle production, in which the magnitude of the correlation in this region is determined by the admixture of charged particles originating from soft and hard processes in the given event selection. The measured particle pair yields support this qualitative argument.

For charged particles with p_{T} above 9 GeV, the v_n results are again consistent between MBT and jet events. Although the uncertainties in the v_3 values make any quantitative statement difficult, v_2 plateaus at a value of 0.025 up to a p_{T} of 50 GeV. This result cannot be explained in the theoretical context of jet quenching or eremitic expansion calculations while simultaneously describing the observed lack of suppression of high-p_{T} hadron and jet yields in p+Pb collisions.

Acknowledgements We thank CERN for the very successful operation of the LHC, as well as the support staff from our institutions without whom ATLAS could not be operated efficiently. We acknowledge the support of ANPCyT, Argentina; YerPhI, Armenia; ARC, Australia; BMWFW and FWF, Austria; ANAS, Azerbaijan; SSTC, Belarus; CNPq and FAPESP, Brazil; NSERC, NRC and CFI, Canada; CERN; CONICYT, Chile; CAS, MOST and NSFC, China; COLCIENCIAS, Colombia; MSMT CR, MPO CR and VSC CR, Czech Republic; DNRF and DNSRC, Denmark; IN2P3-CNRS, CEA-DRF/IRFU, France; SRNSFG, Georgia; BMBF, HGF, and MPG, Germany; GSRT, Greece; RGC, Hong Kong SAR, China; ISF and Benoziyo Center, Israel; INFN, Italy; MEXT and JSPS, Japan; CNRST, Morocco; NWO, Netherlands; RCN, Norway; MNiSW and NCN, Poland; FCT, Portugal; MNE/IFA, Romania; MES of Russia and NRC KI, Russian Federation; JINR; MESTD, Serbia; MSSR, Slovakia; ARRS and MIZŠ, Slovenia; DST/NRF, South Africa; MINECO, Spain; SRC and Wallenberg Foundation, Sweden; SERI, SNSF and Cantons of Bern and Geneva, Switzerland; MOST, Taiwan; TAEK, Turkey; STFC, United Kingdom; DOE and NSF, United States of America. In addition, individual groups and members have received support from BCKDF, CANARIE, CRC and Compute Canada, Canada; COST, ERC, ERDF, Horizon 2020, and Marie Skłodowska-Curie Actions, European Union; Investissements d' Avenir Labex and Idex, ANR, France; DFG and AvH Foundation, Germany; Herakleitos, Thales and Aristeia programmes co-financed by EU-ESF and the Greek NSRF, Greece; BSF-NSF and GIF, Israel; CERCA Programme Generalitat de Catalunya, Spain; The Royal Society and Leverhulme Trust, United Kingdom. The crucial computing support from all WLCG partners is acknowledged gratefully, in particular from CERN, the ATLAS Tier-1 facilities at TRIUMF (Canada), NDGF (Denmark, Norway, Sweden), CC-IN2P3 (France), KIT/GridKA (Germany), INFN-CNAF (Italy), NL-T1 (Netherlands), PIC (Spain), ASGC (Taiwan), RAL (UK) and BNL (USA), the Tier-2 facilities worldwide and large non-WLCG resource providers. Major contributors of computing resources are listed in Ref. [64].

Data Availability Statement This manuscript has no associated data or the data will not be deposited. [Authors' comment: All ATLAS scientific output is published in journals, and preliminary results are made available in Conference Notes. All are openly available, without restriction on use by external parties beyond copyright law and the standard conditions agreed by CERN. Data associated with journal publications are also made available: tables and data from plots (e.g. cross section values, likelihood profiles, selection efficiencies, cross section limits, ...) are stored in appropriate repositories such as HEPDATA (http://hepdata.cedar.ac.uk/). ATLAS also strives to make additional material related to the paper available that allows a reinterpretation of the data in the context of new theoretical models. For example, an extended encapsulation of the analysis is often provided for measurements in the framework of RIVET (http://rivet.hepforge.org/). This information is taken from the ATLAS Data Access Policy, which is a public document that can be downloaded from http://opendata.cern.ch/record/413 [opendata.cern.ch].]

Funded by SCOAP[3].

References

1. U. Heinz, R. Snellings, Collective flow and viscosity in relativistic heavy-ion collisions. Annu. Rev. Nucl. Part. Sci. **63**, 123 (2013)
2. B. Muller, J. Schukraft, B. Wyslouch, First results from $Pb+Pb$ collisions at the LHC. Annu. Rev. Nucl. Part. Sci. **62**, 361 (2012). arXiv:1202.3233 [hep-ex]
3. M. Connors, C. Nattrass, R. Reed, S. Salur, Jet measurements in heavy ion physics. Rev. Mod. Phys. **90**, 025005 (2018). arXiv:1705.01974 [nucl-ex]
4. G.-Y. Qin, X.-N. Wang, Jet quenching in high-energy heavy-ion collisions. Int. J. Mod. Phys. E **24**, 1530014 (2015). arXiv:1511.00790 [hep-ph]
5. Y. Mehtar-Tani, J.G. Milhano, K. Tywoniuk, Jet physics in heavy-ion collisions. Int. J. Mod. Phys. A **28**, 1340013 (2013). arXiv:1302.2579 [hep-ph]
6. J.-P. Blaizot, Y. Mehtar-Tani, Jet structure in heavy ion collisions. Int. J. Mod. Phys. E **24**, 1530012 (2015). arXiv:1503.05958 [hep-ph]
7. CMS Collaboration, Azimuthal anisotropy of charged particles with transverse momentum up to 100 GeV/c in PbPb collisions at $\sqrt{s_{NN}} = 5.02$ TeV. Phys. Lett. B **776**, 195 (2018). arXiv:1702.00630 [hep-ex]
8. ATLAS Collaboration, Measurement of the Azimuthal Angle Dependence of Inclusive Jet Yields in Pb+Pb Collisions at $\sqrt{s_{NN}} = 2.76$ TeV with the ATLAS detector. Phys. Rev. Lett. **111**, 152301 (2013). arXiv:1306.6469 [hep-ex]
9. ALICE Collaboration, Energy dependence and fluctuations of anisotropic flow in Pb-Pb collisions at $\sqrt{s_{NN}} = 5.02$ and 2.76 TeV. JHEP **07**, 103 (2018). arXiv:1804.02944 [nucl-ex]
10. M. Gyulassy, I. Vitev, X.-N. Wang, High p_T azimuthal asymmetry in noncentral A + A at RHIC. Phys. Rev. Lett. **86**, 2537 (2001). 12
11. E.V. Shuryak, Azimuthal asymmetry at large p_t seem to be too large for a pure "jet quenching". Phys. Rev. C **66**, 027902 (2002). arXiv:nucl-th/0112042 [nucl-th]
12. D. Molnar, D. Sun, High-pT suppression and elliptic flow from radiative energy loss with realistic bulk medium expansion (2013). arXiv:1305.1046 [nucl-th]
13. J. Noronha-Hostler, B. Betz, J. Noronha, M. Gyulassy, Event-by-event hydrodynamics + jet energy loss: a solution to the $R_{AA} \bigotimes v_2$ puzzle. Phys. Rev. Lett. **116**, 252301 (2016). 25
14. X. Zhang, J. Liao, Jet quenching and its azimuthal anisotropy in AA and possibly high multiplicity pA and dA collisions (2013). arXiv:1311.5463 [nucl-th]
15. J. Liao, E. Shuryak, Angular dependence of jet quenching indicates its strong enhancement near the QCD phase transition. Phys. Rev. Lett. **102**, 202302 (2009). 20
16. T. Renk, On the sensitivity of jet quenching to near T_C enhancement of the medium opacity. Phys. Rev. C **89**, 067901 (2014). arXiv:1402.5798 [hep-ph]

17. B.Z. Kopeliovich, J. Nemchik, I.K. Potashnikova, I. Schmidt, Quenching of high-p_T hadrons: energy loss versus color transparency. Phys. Rev. C **86**, 054904 (2012). 5
18. ATLAS Collaboration, Observation of associated near-side and away-side long-range correlations in $\sqrt{s_{NN}} = 5.02$ TeV proton-lead collisions with the ATLAS detector. Phys. Rev. Lett. **110**, 182302 (2013). arXiv:1212.5198 [hep-ex]
19. ATLAS Collaboration, Measurements of long-range azimuthal anisotropies and associated Fourier coefficients for pp collisions at $\sqrt{s} = 5.02$ and 13 TeV and p+Pb collisions at $\sqrt{s_{NN}} = 5.02$ TeV with the ATLAS detector. Phys. Rev. C **96**, 024908 (2017). arXiv:1609.06213 [hep-ex]
20. ATLAS Collaboration, Observation of long-range elliptic azimuthal anisotropies in $\sqrt{s} = 13$ and 2.76 TeV pp collisions with the ATLAS detector. Phys. Rev. Lett. **116**, 172301 (2016). arXiv:1509.04776 [hep-ex]
21. CMS Collaboration, Observation of long-range, near-side angular correlations in proton–proton collisions at the LHC. JHEP **09**, 091 (2010). arXiv:1009.4122 [hep-ex]
22. CMS Collaboration, Evidence for collective multiparticle correlations in pPb collisions. Phys. Rev. Lett. **115**, 012301 (2015). arXiv:1502.05382 [hep-ex]
23. ALICE Collaboration, Multiplicity dependence of the average transverse momentum in pp, p-Pb, and Pb-Pb collisions at the LHC. Phys. Lett. B **727**, 371 (2013). arXiv:1307.1094 [nucl-ex]
24. PHENIX Collaboration, Creation of quark-gluon plasma droplets with three distinct geometries. Nat. Phys. **15**, 214 (2019) . arXiv:1805.02973 [nucl-ex]
25. J.L. Nagle, W.A. Zajc, Small system collectivity in relativistic hadronic and nuclear collisions. Annu. Rev. Nucl. Part. Sci. **68**, 211 (2018). arXiv:1801.03477 [nucl-ex]
26. P. Romatschke, U. Romatschke, Relativistic fluid dynamics in and out of equilibrium, Cambridge Monographs on Mathematical Physics. Cambridge University Press, Cambridge (2019). arXiv:1712.05815 [nucl-th]
27. ATLAS Collaboration, Centrality and rapidity dependence of inclusive jet production in $\sqrt{s_{NN}} = 5.02$ TeV proton-lead collisions with the ATLAS detector. Phys. Lett. B **748** 392 (2015). arXiv:1412.4092 [hep-ex]
28. CMS Collaboration, Measurement of inclusive jet production and nuclear modifications in pPb collisions at $\sqrt{s_{NN}} = 5.02$ TeV. Eur. Phys. J. C **76**, 372 (2016). arXiv:1601.02001 [hep-ex]
29. ALICE Collaboration, Transverse momentum distribution and nuclear modification factor of charged particles in p+Pb collisions at $\sqrt{s_{NN}} = 5.02$ TeV. Phys. Rev. Lett. **110**, 082302 (2013). arXiv:1210.4520 [nucl-ex]
30. PHENIX Collaboration, Centrality-dependent modification of jet-production rates in deuteron-gold collisions at $\sqrt{s_{NN}} = 200$ GeV. Phys. Rev. Lett. **116**, 122301, (2016). arXiv:1509.04657 [nucl-ex]
31. CMS Collaboration, Studies of dijet transverse momentum balance and pseudorapidity distributions in pPb collisions at $\sqrt{s_{NN}} = 5.02$ TeV. Eur. Phys. J. C **74**, 2951 (2014). arXiv:1401.4433 [hep-ex]
32. ALICE Collaboration, Constraints on jet quenching in p-Pb collisions at $\sqrt{s_{NN}} = 5.02$ TeV measured by the event-activity dependence of semi-inclusive hadron-jet distributions. Phys. Lett. B **783**, 95 (2018). arXiv:1712.05603 [nucl-ex]
33. ATLAS Collaboration, Measurement of long-range pseudorapidity correlations and azimuthal harmonics in $\sqrt{s_{NN}} = 5.02$ TeV proton-lead collisions with the ATLAS detector. Phys. Rev. C **90**, 044906 (2014). arXiv:1409.1792 [hep-ex]
34. S.H. Lim et al., Examination of flow and nonflow factorization methods in small collision systems. Phys. Rev. C **100**, 024908 (2019). 2
35. ATLAS Collaboration, The ATLAS Experiment at the CERN Large Hadron Collider, JINST **3**, S08003 (2008)
36. ATLAS Collaboration, ATLAS Insertable B-Layer Technical Design Report, ATLAS-TDR-19 (2010), https://cds.cern.ch/record/1291633, ATLAS insertable B-layer technical design report addendum, ATLAS-TDR-19-ADD-1 (2012), https://cds.cern.ch/record/1451888
37. B. Abbott et al., Production and integration of the ATLAS Insertable B-Layer. JINST **13**, T05008 (2018). arXiv:1803.00844 [physics.ins-det]
38. ATLAS Collaboration, Performance of the ATLAS trigger system in 2015. Eur. Phys. J. C **77**, 317 (2017). arXiv:1611.09661 [hep-ex]
39. ATLAS Collaboration, Track reconstruction performance of the ATLAS inner detector at $\sqrt{s} = 13$ TeV, ATL-PHYS-PUB-2015-018 (2015). https://cds.cern.ch/record/2037683
40. ATLAS Collaboration, Measurement of the centrality dependence of the charged-particle pseudorapidity distribution in proton-lead collisions at $\sqrt{s_{NN}} = 5.02$ TeV with the ATLAS detector. Eur. Phys. J. C **76**, 199 (2016). arXiv:1508.00848 [hep-ex]
41. J. Adam et al., Centrality dependence of particle production in p-Pb collisions at $\sqrt{s_{NN}} = 5.02$ TeV. Phys. Rev. C **91**, 064905 (2015). arXiv:1412.6828 [nucl-ex]
42. ATLAS Collaboration, Study of the material of the ATLAS inner detector for Run 2 of the LHC. JINST **12**, P12009 (2017). arXiv:1707.02826 [hep-ex]
43. W.-T. Deng, X.-N. Wang and R. Xu, Hadron production in p+p, p+Pb, and Pb+Pb collisions with the HIJING 2.0 model at energies available at the CERN Large Hadron Collider. Phys. Rev. C **83**, 014915 (2011). arXiv:1008.1841 [hep-ph]
44. S. Agostinelli et al., GEANT4—a simulation toolkit. Nucl. Instrum. Methods A **506**, 250 (2003)
45. ATLAS Collaboration, The ATLAS simulation infrastructure. Eur. Phys. J. C **70**, 823 (2010). arXiv:1005.4568 [physics.ins-det]
46. ATLAS Collaboration, Measurement of the jet radius and transverse momentum dependence of inclusive jet suppression in lead-lead collisions at $\sqrt{s_{NN}} = 2.76$ TeV with the ATLAS detector. Phys. Lett. B **719**, 220 (2013). arXiv:1208.1967 [hep-ex]
47. ATLAS Collaboration, Measurement of jet fragmentation in Pb+Pb and pp collisions at $\sqrt{s_{NN}} = 5.02$ TeV with the ATLAS detector. Phys. Rev. C **98**, 024908 (2018). arXiv:1805.05424 [hep-ex]
48. M. Cacciari, G.P. Salam, G. Soyez, The $anti\text{-}k_t$ jet clustering algorithm. JHEP **04**, 063 (2008). arXiv:0802.1189 [hep-ph]
49. M. Cacciari, G.P. Salam, G. Soyez, FastJet user manual. Eur. Phys. J. C **72**, 1896 (2012)
50. T. Sjöstrand et al., An introduction to PYTHIA 8.2. Comput. Phys. Commun. **191**, 159 (2015). arXiv:1410.3012 [hep-ph]
51. R.D. Ball et al., Parton distributions with LHC data. Nucl. Phys. B **867**, 244 (2013). arXiv:1207.1303 [hep-ph]
52. ATLAS Collaboration, ATLAS Pythia 8 tunes to 7 TeV data, ATL-PHYS-PUB-2014-021 (2014). https://cds.cern.ch/record/1966419
53. ATLAS Collaboration, Jet energy scale measurements and their systematic uncertainties in proton-proton collisions at $\sqrt{s} = 13$ TeV with the ATLAS detector. Phys. Rev. D **96**, 072002 (2017). arXiv:1703.09665 [hep-ex]
54. ATLAS Collaboration, Measurement of photon-jet transverse momentum correlations in 5.02 TeV Pb+Pb and pp collisions with ATLAS. Phys. Lett. B **789**, 167 (2019). arXiv:1809.07280 [hep-ex]
55. F. James, M. Roos, Minuit—a system for function minimization and analysis of the parameter errors and correlations. Comput. Phys. Commun. **10**, 343 (1975)
56. M.L. Miller, K. Reygers, S.J. Sanders, P. Steinberg, Glauber modeling in high energy nuclear collisions. Annu. Rev. Nucl. Part. Sci. **57**, 205 (2007). arXiv:nucl-ex/0701025 [nucl-ex]
57. ATLAS Collaboration, Transverse momentum, rapidity, and centrality dependence of inclusive charged-particle production in $\sqrt{s_{NN}} = 5.02$ TeV p+Pb collisions measured by the ATLAS experiment. Phys. Lett. B **763**, 313 (2016). arXiv:1605.06436 [hep-ex]

58. H. Mäntysaari, B. Schenke, C. Shen, P. Tribedy, Imprints of fluctuating proton shapes on flow in proton-lead collisions at the LHC. Phys. Lett. B **772**, 681 (2017). arXiv:1705.03177 [nucl-th]
59. R.D. Weller, P. Romatschke, One fluid to rule them all: viscous hydrodynamic description of event-by-event central p+p, p+Pb and Pb+Pb collisions at $\sqrt{s} = 5.02$ TeV. Phys. Lett. B **774**, 351 (2017). arXiv:1701.07145 [nucl-th]
60. C. Bierlich, G. Gustafson, L. Lönnblad, H. Shah, The Angantyr model for heavy-ion collisions in PYTHIA8. JHEP **10**, 134 (2018). arXiv:1806.10820 [hep-ph]
61. C. Bierlich, Microscopic collectivity: The ridge and strangeness enhancement from string-string interactions. Nucl. Phys. A **982**, 499 (2019). The 27th International Conference on Ultrarelativistic Nucleus-Nucleus Collisions: Quark Matter 2018
62. ATLAS Collaboration, Measurement of the azimuthal anisotropy of charged particles produced in $\sqrt{s_{NN}} = 5.02$ TeV Pb+Pb collisions with the ATLAS detector. Eur. Phys. J. C **78**, 997 (2018). arXiv:1808.03951 [hep-ex]
63. C. Loizides, J. Kamin, D. d'Enterria, Improved Monte Carlo Glauber predictions at present and future nuclear colliders. Phys. Rev. C **97**, 054910 (2018). arXiv:1710.07098 [nucl-ex], Erratum: Phys. Rev. C 99
64. ATLAS Collaboration, ATLAS Computing Acknowledgements, ATL-GEN-PUB-2016-002. https://cds.cern.ch/record/2202407

ATLAS Collaboration

G. Aad[101], B. Abbott[128], D. C. Abbott[102], A. Abed Abud[36], K. Abeling[53], D. K. Abhayasinghe[93], S. H. Abidi[167], O. S. AbouZeid[40], N. L. Abraham[156], H. Abramowicz[161], H. Abreu[160], Y. Abulaiti[6], B. S. Acharya[66a,66b,n], B. Achkar[53], S. Adachi[163], L. Adam[99], C. Adam Bourdarios[5], L. Adamczyk[83a], L. Adamek[167], J. Adelman[120], M. Adersberger[113], A. Adiguzel[12c], S. Adorni[54], T. Adye[144], A. A. Affolder[146], Y. Afik[160], C. Agapopoulou[132], M. N. Agaras[38], A. Aggarwal[118], C. Agheorghiesei[27c], J. A. Aguilar-Saavedra[140a,140f,ae], F. Ahmadov[79], W. S. Ahmed[103], X. Ai[18], G. Aielli[73a,73b], S. Akatsuka[85], T. P. A. Åkesson[96], E. Akilli[54], A. V. Akimov[110], K. Al Khoury[132], G. L. Alberghi[23a,23b], J. Albert[176], M. J. Alconada Verzini[161], S. Alderweireldt[36], M. Aleksa[36], I. N. Aleksandrov[79], C. Alexa[27b], T. Alexopoulos[10], A. Alfonsi[119], F. Alfonsi[23a,23b], M. Alhroob[128], B. Ali[142], M. Aliev[166], G. Alimonti[68a], C. Allaire[132], B. M. M. Allbrooke[156], B. W. Allen[131], P. P. Allport[21], A. Aloisio[69a,69b], F. Alonso[88], C. Alpigiani[148], A. A. Alshehri[57], M. Alvarez Estevez[98], M. G. Alviggi[69a,69b], Y. Amaral Coutinho[80b], A. Ambler[103], L. Ambroz[135], C. Amelung[26], D. Amidei[105], S. P. Amor Dos Santos[140a], S. Amoroso[46], C. S. Amrouche[54], F. An[78], C. Anastopoulos[149], N. Andari[145], T. Andeen[11], C. F. Anders[61b], J. K. Anders[20], A. Andreazza[68a,68b], V. Andrei[61a], C. R. Anelli[176], S. Angelidakis[38], A. Angerami[39], A. V. Anisenkov[121a,121b], A. Annovi[71a], C. Antel[54], M. T. Anthony[149], E. Antipov[129], M. Antonelli[51], D. J. A. Antrim[171], F. Anulli[72a], M. Aoki[81], J. A. Aparisi Pozo[174], L. Aperio Bella[15a], J. P. Araque[140a], V. Araujo Ferraz[80b], R. Araujo Pereira[80b], C. Arcangeletti[51], A. T. H. Arce[49], F. A. Arduh[88], J.-F. Arguin[109], S. Argyropoulos[52], J.-H. Arling[46], A. J. Armbruster[36], A. Armstrong[171], O. Arnaez[167], H. Arnold[119], Z. P. Arrubarrena Tame[113], G. Artoni[135], S. Artz[99], S. Asai[163], T. Asawatavonvanich[165], N. Asbah[59], E. M. Asimakopoulou[172], L. Asquith[156], J. Assahsah[35d], K. Assamagan[29], R. Astalos[28a], R. J. Atkin[33a], M. Atkinson[173], N. B. Atlay[19], H. Atmani[132], K. Augsten[142], G. Avolio[36], M. K. Ayoub[15a], G. Azuelos[109,ap], H. Bachacou[145], K. Bachas[67a,67b], M. Backes[135], F. Backman[45a,45b], P. Bagnaia[72a,72b], M. Bahmani[84], H. Bahrasemani[152], A. J. Bailey[174], V. R. Bailey[173], J. T. Baines[144], C. Bakalis[10], O. K. Baker[183], P. J. Bakker[119], D. Bakshi Gupta[8], S. Balaji[157], E. M. Baldin[121a,121b], P. Balek[180], F. Balli[145], W. K. Balunas[135], J. Balz[99], E. Banas[84], A. Bandyopadhyay[24], Sw. Banerjee[181,i], A. A. E. Bannoura[182], L. Barak[161], W. M. Barbe[38], E. L. Barberio[104], D. Barberis[55a,55b], M. Barbero[101], G. Barbour[94], T. Barillari[114], M.-S. Barisits[36], J. Barkeloo[131], T. Barklow[153], R. Barnea[160], B. M. Barnett[144], R. M. Barnett[18], Z. Barnovska-Blenessy[60a], A. Baroncelli[60a], G. Barone[29], A. J. Barr[135], L. Barranco Navarro[45a,45b], F. Barreiro[98], J. Barreiro Guimarães da Costa[15a], S. Barsov[138], R. Bartoldus[153], G. Bartolini[101], A. E. Barton[89], P. Bartos[28a], A. Basalaev[46], A. Basan[99], A. Bassalat[132,ak], M. J. Basso[167], R. L. Bates[57], S. Batlamous[35e], J. R. Batley[32], B. Batool[151], M. Battaglia[146], M. Bauce[72a,72b], F. Bauer[145], K. T. Bauer[171], H. S. Bawa[31], J. B. Beacham[49], T. Beau[136], P. H. Beauchemin[170], F. Becherer[52], P. Bechtle[24], H. C. Beck[53], H. P. Beck[20,r], K. Becker[178], C. Becot[46], A. Beddall[12d], A. J. Beddall[12a], V. A. Bednyakov[79], M. Bedognetti[119], C. P. Bee[155], T. A. Beermann[182], M. Begalli[80b], M. Begel[29], A. Behera[155], J. K. Behr[46], F. Beisiegel[24], A. S. Bell[94], G. Bella[161], L. Bellagamba[23b], A. Bellerive[34], P. Bellos[9], K. Beloborodov[121a,121b], K. Belotskiy[111], N. L. Belyaev[111], D. Benchekroun[35a], N. Benekos[10], Y. Benhammou[161], D. P. Benjamin[6], M. Benoit[54], J. R. Bensinger[26], S. Bentvelsen[119], L. Beresford[135], M. Beretta[51], D. Berge[19], E. Bergeaas Kuutmann[172], N. Berger[5], B. Bergmann[142], L. J. Bergsten[26], J. Beringer[18], S. Berlendis[7], G. Bernardi[136], C. Bernius[153], F. U. Bernlochner[24], T. Berry[93], P. Berta[99], C. Bertella[15a], I. A. Bertram[89], O. Bessidskaia Bylund[182], N. Besson[145], A. Bethani[100], S. Bethke[114], A. Betti[42], A. J. Bevan[92], J. Beyer[114], D. S. Bhattacharya[177], P. Bhattarai[26], R. Bi[139], R. M. Bianchi[139], O. Biebel[113], D. Biedermann[19], R. Bielski[36], K. Bierwagen[99], N. V. Biesuz[71a,71b], M. Biglietti[74a], T. R. V. Billoud[109], M. Bindi[53], A. Bingul[12d], C. Bini[72a,72b], S. Biondi[23a,23b], M. Birman[180], T. Bisanz[53], J. P. Biswal[3], D. Biswas[181,i], A. Bitadze[100], C. Bittrich[48], K. Bjørke[134], T. Blazek[28a], I. Bloch[46], C. Blocker[26], A. Blue[57], U. Blumenschein[92], G. J. Bobbink[119], V. S. Bobrovnikov[121a,121b],

S. S. Bocchetta[96], A. Bocci[49], D. Boerner[46], D. Bogavac[14], A. G. Bogdanchikov[121a,121b], C. Bohm[45a], V. Boisvert[93], P. Bokan[53], T. Bold[83a], A. E. Bolz[61b], M. Bomben[136], M. Bona[92], J. S. Bonilla[131], M. Boonekamp[145], C. D. Booth[93], H. M. Borecka-Bielska[90], L. S. Borgna[94], A. Borisov[122], G. Borissov[89], J. Bortfeldt[36], D. Bortoletto[135], D. Boscherini[23b], M. Bosman[14], J. D. Bossio Sola[103], K. Bouaouda[35a], J. Boudreau[139], E. V. Bouhova-Thacker[89], D. Boumediene[38], S. K. Boutle[57], A. Boveia[126], J. Boyd[36], D. Boye[33b,al], I. R. Boyko[79], A. J. Bozson[93], J. Bracinik[21], N. Brahimi[101], G. Brandt[182], O. Brandt[32], F. Braren[46], B. Brau[102], J. E. Brau[131], W. D. Breaden Madden[57], K. Brendlinger[46], L. Brenner[46], R. Brenner[172], S. Bressler[180], B. Brickwedde[99], D. L. Briglin[21], D. Britton[57], D. Britzger[114], I. Brock[24], R. Brock[106], G. Brooijmans[39], W. K. Brooks[147c], E. Brost[29], J. H. Broughton[21], P. A. Bruckman de Renstrom[84], D. Bruncko[28b], A. Bruni[23b], G. Bruni[23b], L. S. Bruni[119], S. Bruno[73a,73b], M. Bruschi[23b], N. Bruscino[72a,72b], P. Bryant[37], L. Bryngemark[96], T. Buanes[17], Q. Buat[36], P. Buchholz[151], A. G. Buckley[57], I. A. Budagov[79], M. K. Bugge[134], F. Bührer[52], O. Bulekov[111], T. J. Burch[120], S. Burdin[90], C. D. Burgard[119], A. M. Burger[129], B. Burghgrave[8], J. T. P. Burr[46], C. D. Burton[11], J. C. Burzynski[102], V. Büscher[99], E. Buschmann[53], P. J. Bussey[57], J. M. Butler[25], C. M. Buttar[57], J. M. Butterworth[94], P. Butti[36], W. Buttinger[36], C. J. Buxo Vazquez[106], A. Buzatu[158], A. R. Buzykaev[121a,121b], G. Cabras[23a,23b], S. Cabrera Urbán[174], D. Caforio[56], H. Cai[173], V. M. M. Cairo[153], O. Cakir[4a], N. Calace[36], P. Calafiura[18], A. Calandri[101], G. Calderini[136], P. Calfayan[65], G. Callea[57], L. P. Caloba[80b], A. Caltabiano[73a,73b], S. Calvente Lopez[98], D. Calvet[38], S. Calvet[38], T. P. Calvet[155], M. Calvetti[71a,71b], R. Camacho Toro[136], S. Camarda[36], D. Camarero Munoz[98], P. Camarri[73a,73b], D. Cameron[134], C. Camincher[36], S. Campana[36], M. Campanelli[94], A. Camplani[40], A. Campoverde[151], V. Canale[69a,69b], A. Canesse[103], M. Cano Bret[60c], J. Cantero[129], T. Cao[161], Y. Cao[173], M. D. M. Capeans Garrido[36], M. Capua[41a,41b], R. Cardarelli[73a], F. Cardillo[149], G. Carducci[41a,41b], I. Carli[143], T. Carli[36], G. Carlino[69a], B. T. Carlson[139], L. Carminati[68a,68b], R. M. D. Carney[153], S. Caron[118], E. Carquin[147c], S. Carrá[46], J. W. S. Carter[167], M. P. Casado[14,e], A. F. Casha[167], R. Castelijn[119], F. L. Castillo[174], L. Castillo Garcia[14], V. Castillo Gimenez[174], N. F. Castro[140a,140e], A. Catinaccio[36], J. R. Catmore[134], A. Cattai[36], V. Cavaliere[29], E. Cavallaro[14], M. Cavalli-Sforza[14], V. Cavasinni[71a,71b], E. Celebi[12b], L. Cerda Alberich[174], K. Cerny[130], A. S. Cerqueira[80a], A. Cerri[156], L. Cerrito[73a,73b], F. Cerutti[18], A. Cervelli[23a,23b], S. A. Cetin[12b], Z. Chadi[35a], D. Chakraborty[120], J. Chan[181], W. S. Chan[119], W. Y. Chan[90], J. D. Chapman[32], B. Chargeishvili[159b], D. G. Charlton[21], T. P. Charman[92], C. C. Chau[34], S. Che[126], S. Chekanov[6], S. V. Chekulaev[168a], G. A. Chelkov[79,ao], B. Chen[78], C. Chen[60a], C. H. Chen[78], H. Chen[29], J. Chen[60a], J. Chen[39], J. Chen[26], S. Chen[137], S. J. Chen[15c], X. Chen[15b], Y.-H. Chen[46], H. C. Cheng[63a], H. J. Cheng[15a], A. Cheplakov[79], E. Cheremushkina[122], R. Cherkaoui El Moursli[35e], E. Cheu[7], K. Cheung[64], T. J. A. Chevalérias[145], L. Chevalier[145], V. Chiarella[51], G. Chiarelli[71a], G. Chiodini[67a], A. S. Chisholm[21], A. Chitan[27b], I. Chiu[163], Y. H. Chiu[176], M. V. Chizhov[79], K. Choi[11], A. R. Chomont[72a,72b], S. Chouridou[162], Y. S. Chow[119], M. C. Chu[63a], X. Chu[15a,15d], J. Chudoba[141], J. J. Chwastowski[84], L. Chytka[130], D. Cieri[114], K. M. Ciesla[84], D. Cinca[47], V. Cindro[91], I. A. Cioară[27b], A. Ciocio[18], F. Cirotto[69a,69b], Z. H. Citron[180,j], M. Citterio[68a], D. A. Ciubotaru[27b], B. M. Ciungu[167], A. Clark[54], M. R. Clark[39], P. J. Clark[50], C. Clement[45a,45b], Y. Coadou[101], M. Cobal[66a,66c], A. Coccaro[55b], J. Cochran[78], H. Cohen[161], A. E. C. Coimbra[36], B. Cole[39], A. P. Colijn[119], J. Collot[58], P. Conde Muiño[140a,140h], S. H. Connell[33b], I. A. Connelly[57], S. Constantinescu[27b], F. Conventi[69a,aq], A. M. Cooper-Sarkar[135], F. Cormier[175], K. J. R. Cormier[167], L. D. Corpe[94], M. Corradi[72a,72b], E. E. Corrigan[96], F. Corriveau[103,ac], A. Cortes-Gonzalez[36], M. J. Costa[174], F. Costanza[5], D. Costanzo[149], G. Cowan[93], J. W. Cowley[32], J. Crane[100], K. Cranmer[124], S. J. Crawley[57], R. A. Creager[137], S. Crépé-Renaudin[58], F. Crescioli[136], M. Cristinziani[24], V. Croft[170], G. Crosetti[41a,41b], A. Cueto[5], T. Cuhadar Donszelmann[149], A. R. Cukierman[153], W. R. Cunningham[57], S. Czekierda[84], P. Czodrowski[36], M. J. Da Cunha Sargedas De Sousa[60b], J. V. Da Fonseca Pinto[80b], C. Da Via[100], W. Dabrowski[83a], F. Dachs[36], T. Dado[28a], S. Dahbi[33d], T. Dai[105], C. Dallapiccola[102], M. Dam[40], G. D'amen[29], V. D'Amico[74a,74b], J. Damp[99], J. R. Dandoy[137], M. F. Daneri[30], N. S. Dann[100], M. Danninger[152], V. Dao[36], G. Darbo[55b], O. Dartsi[5], A. Dattagupta[131], T. Daubney[46], S. D'Auria[68a,68b], C. David[168b], T. Davidek[143], D. R. Davis[49], I. Dawson[149], K. De[8], R. De Asmundis[69a], M. De Beurs[119], S. De Castro[23a,23b], S. De Cecco[72a,72b], N. De Groot[118], P. de Jong[119], H. De la Torre[106], A. De Maria[15c], D. De Pedis[72a], A. De Salvo[72a], U. De Sanctis[73a,73b], M. De Santis[73a,73b], A. De Santo[156], K. De Vasconcelos Corga[101], J. B. De Vivie De Regie[132], C. Debenedetti[146], D. V. Dedovich[79], A. M. Deiana[42], J. Del Peso[98], Y. Delabat Diaz[46], D. Delgove[132], F. Deliot[145,q], C. M. Delitzsch[7], M. Della Pietra[69a,69b], D. Della Volpe[54], A. Dell'Acqua[36], L. Dell'Asta[73a,73b], M. Delmastro[5], C. Delporte[132], P. A. Delsart[58], D. A. DeMarco[167], S. Demers[183], M. Demichev[79], G. Demontigny[109], S. P. Denisov[122], L. D'Eramo[136], D. Derendarz[84], J. E. Derkaoui[35d], F. Derue[136], P. Dervan[90], K. Desch[24], C. Deterre[46], K. Dette[167], C. Deutsch[24], M. R. Devesa[30], P. O. Deviveiros[36], F. A. Di Bello[72a,72b], A. Di Ciaccio[73a,73b], L. Di Ciaccio[5], W. K. Di Clemente[137], C. Di Donato[69a,69b], A. Di Girolamo[36], G. Di Gregorio[71a,71b], B. Di Micco[74a,74b], R. Di Nardo[74a,74b], K. F. Di Petrillo[59], R. Di Sipio[167], C. Diaconu[101], F. A. Dias[40], T. Dias Do Vale[140a], M. A. Diaz[147a], J. Dickinson[18], E. B. Diehl[105], J. Dietrich[19], S. Díez Cornell[46], A. Dimitrievska[18], W. Ding[15b], J. Dingfelder[24], F. Dittus[36], F. Djama[101], T. Djobava[159b],

J. I. Djuvsland[17], M. A. B. Do Vale[80c], M. Dobre[27b], D. Dodsworth[26], C. Doglioni[96], J. Dolejsi[143], Z. Dolezal[143], M. Donadelli[80d], B. Dong[60c], J. Donini[38], A. D'onofrio[15c], M. D'Onofrio[90], J. Dopke[144], A. Doria[69a], M. T. Dova[88], A. T. Doyle[57], E. Drechsler[152], E. Dreyer[152], T. Dreyer[53], A. S. Drobac[170], D. Du[60b], Y. Duan[60b], F. Dubinin[110], M. Dubovsky[28a], A. Dubreuil[54], E. Duchovni[180], G. Duckeck[113], A. Ducourthial[136], O. A. Ducu[109], D. Duda[114], A. Dudarev[36], A. C. Dudder[99], E. M. Duffield[18], L. Duflot[132], M. Dührssen[36], C. Dülsen[182], M. Dumancic[180], A. E. Dumitriu[27b], A. K. Duncan[57], M. Dunford[61a], A. Duperrin[101], H. Duran Yildiz[4a], M. Düren[56], A. Durglishvili[159b], D. Duschinger[48], B. Dutta[46], D. Duvnjak[1], G. I. Dyckes[137], M. Dyndal[36], S. Dysch[100], B. S. Dziedzic[84], K. M. Ecker[114], M. G. Eggleston[49], T. Eifert[8], G. Eigen[17], K. Einsweiler[18], T. Ekelof[172], H. El Jarrari[35e], R. El Kosseifi[101], V. Ellajosyula[172], M. Ellert[172], F. Ellinghaus[182], A. A. Elliot[92], N. Ellis[36], J. Elmsheuser[29], M. Elsing[36], D. Emeliyanov[144], A. Emerman[39], Y. Enari[163], M. B. Epland[49], J. Erdmann[47], A. Ereditato[20], P. A. Erland[84], M. Errenst[36], M. Escalier[132], C. Escobar[174], O. Estrada Pastor[174], E. Etzion[161], H. Evans[65], A. Ezhilov[138], F. Fabbri[57], L. Fabbri[23a,23b], V. Fabiani[118], G. Facini[178], R. M. Faisca Rodrigues Pereira[140a], R. M. Fakhrutdinov[122], S. Falciano[72a], P. J. Falke[5], S. Falke[5], J. Faltova[143], Y. Fang[15a], Y. Fang[15a], G. Fanourakis[44], M. Fanti[68a,68b], M. Faraj[66a,66c,s], A. Farbin[8], A. Farilla[74a], E. M. Farina[70a,70b], T. Farooque[106], S. M. Farrington[50], P. Farthouat[36], F. Fassi[35e], P. Fassnacht[36], D. Fassouliotis[9], M. Faucci Giannelli[50], W. J. Fawcett[32], L. Fayard[132], O. L. Fedin[138,o], W. Fedorko[175], A. Fehr[20], M. Feickert[173], L. Feligioni[101], A. Fell[149], C. Feng[60b], M. Feng[49], M. J. Fenton[171], A. B. Fenyuk[122], S. W. Ferguson[43], J. Ferrando[46], A. Ferrante[173], A. Ferrari[172], P. Ferrari[119], R. Ferrari[70a], D. E. Ferreira de Lima[61b], A. Ferrer[174], D. Ferrere[54], C. Ferretti[105], F. Fiedler[99], A. Filipčič[91], F. Filthaut[118], K. D. Finelli[25], M. C. N. Fiolhais[140a,140c,a], L. Fiorini[174], F. Fischer[113], W. C. Fisher[106], I. Fleck[151], P. Fleischmann[105], T. Flick[182], B. M. Flierl[113], L. Flores[137], L. R. Flores Castillo[63a], F. M. Follega[75a,75b], N. Fomin[17], J. H. Foo[167], G. T. Forcolin[75a,75b], A. Formica[145], F. A. Förster[14], A. C. Forti[100], A. G. Foster[21], M. G. Foti[135], D. Fournier[132], H. Fox[89], P. Francavilla[71a,71b], S. Francescato[72a,72b], M. Franchini[23a,23b], S. Franchino[61a], D. Francis[36], L. Franconi[20], M. Franklin[59], A. N. Fray[92], P. M. Freeman[21], B. Freund[109], W. S. Freund[80b], E. M. Freundlich[47], D. C. Frizzell[128], D. Froidevaux[36], J. A. Frost[135], C. Fukunaga[164], E. Fullana Torregrosa[174], T. Fusayasu[115], J. Fuster[174], A. Gabrielli[23a,23b], A. Gabrielli[18], S. Gadatsch[54], P. Gadow[114], G. Gagliardi[55a,55b], L. G. Gagnon[109], B. Galhardo[140a], G. E. Gallardo[135], E. J. Gallas[135], B. J. Gallop[144], G. Galster[40], R. Gamboa Goni[92], K. K. Gan[126], S. Ganguly[180], J. Gao[60a], Y. Gao[50], Y. S. Gao[31,l], C. García[174], J. E. García Navarro[174], J. A. García Pascual[15a], C. Garcia-Argos[52], M. Garcia-Sciveres[18], R. W. Gardner[37], N. Garelli[153], S. Gargiulo[52], C. A. Garner[167], V. Garonne[134], S. J. Gasiorowski[148], P. Gaspar[80b], A. Gaudiello[55a,55b], G. Gaudio[70a], I. L. Gavrilenko[110], A. Gavrilyuk[123], C. Gay[175], G. Gaycken[46], E. N. Gazis[10], A. A. Geanta[27b], C. M. Gee[146], C. N. P. Gee[144], J. Geisen[96], M. Geisen[99], C. Gemme[55b], M. H. Genest[58], C. Geng[105], S. Gentile[72a,72b], S. George[93], T. Geralis[44], L. O. Gerlach[53], P. Gessinger-Befurt[99], G. Gessner[47], S. Ghasemi[151], M. Ghasemi Bostanabad[176], M. Ghneimat[151], A. Ghosh[132], A. Ghosh[77], B. Giacobbe[23b], S. Giagu[72a,72b], N. Giangiacomi[23a,23b], P. Giannetti[71a], A. Giannini[69a,69b], G. Giannini[14], S. M. Gibson[93], M. Gignac[146], D. Gillberg[34], G. Gilles[182], D. M. Gingrich[3,ap], M. P. Giordani[66a,66c], P. F. Giraud[145], G. Giugliarelli[66a,66c], D. Giugni[68a], F. Giuli[73a,73b], S. Gkaitatzis[162], I. Gkialas[9,g], E. L. Gkougkousis[14], P. Gkountoumis[10], L. K. Gladilin[112], C. Glasman[98], J. Glatzer[14], P. C. F. Glaysher[46], A. Glazov[46], G. R. Gledhill[131], M. Goblirsch-Kolb[26], D. Godin[109], S. Goldfarb[104], T. Golling[54], D. Golubkov[122], A. Gomes[140a,140b], R. Goncalves Gama[53], R. Gonçalo[140a,140b], G. Gonella[131], L. Gonella[21], A. Gongadze[79], F. Gonnella[21], J. L. Gonski[39], S. González de la Hoz[174], S. Gonzalez Fernandez[14], S. Gonzalez-Sevilla[54], G. R. Gonzalvo Rodriguez[174], L. Goossens[36], N. A. Gorasia[21], P. A. Gorbounov[123], H. A. Gordon[29], B. Gorini[36], E. Gorini[67a,67b], A. Gorišek[91], A. T. Goshaw[49], M. I. Gostkin[79], C. A. Gottardo[118], M. Gouighri[35b], A. G. Goussiou[148], N. Govender[33b], C. Goy[5], E. Gozani[160], I. Grabowska-Bold[83a], E. C. Graham[90], J. Gramling[171], E. Gramstad[134], S. Grancagnolo[19], M. Grandi[156], V. Gratchev[138], P. M. Gravila[27f], F. G. Gravili[67a,67b], C. Gray[57], H. M. Gray[18], C. Grefe[24], K. Gregersen[96], I. M. Gregor[46], P. Grenier[153], K. Grevtsov[46], C. Grieco[14], N. A. Grieser[128], A. A. Grillo[146], K. Grimm[31,k], S. Grinstein[14,x], J.-F. Grivaz[132], S. Groh[99], E. Gross[180], J. Grosse-Knetter[53], Z. J. Grout[94], C. Grud[105], A. Grummer[117], L. Guan[105], W. Guan[181], C. Gubbels[175], J. Guenther[36], A. Guerguichon[132], J. G. R. Guerrero Rojas[174], F. Guescini[114], D. Guest[171], R. Gugel[52], T. Guillemin[5], S. Guindon[36], U. Gul[57], J. Guo[60c], W. Guo[105], Y. Guo[60a], Z. Guo[101], R. Gupta[46], S. Gurbuz[12c], G. Gustavino[128], M. Guth[52], P. Gutierrez[128], C. Gutschow[94], C. Guyot[145], C. Gwenlan[135], C. B. Gwilliam[90], A. Haas[124], C. Haber[18], H. K. Hadavand[8], A. Hadef[60a], M. Haleem[177], J. Haley[129], G. Halladjian[106], G. D. Hallewell[101], K. Hamacher[182], P. Hamal[130], K. Hamano[176], H. Hamdaoui[35e], M. Hamer[24], G. N. Hamity[50], K. Han[60a,ag], L. Han[60a], S. Han[15a], Y. F. Han[167], K. Hanagaki[81,v], M. Hance[146], D. M. Handl[113], B. Haney[137], R. Hankache[136], E. Hansen[96], J. B. Hansen[40], J. D. Hansen[40], M. C. Hansen[24], P. H. Hansen[40], E. C. Hanson[100], K. Hara[169], T. Harenberg[182], S. Harkusha[107], P. F. Harrison[178], N. M. Hartmann[113], Y. Hasegawa[150], A. Hasib[50], S. Hassani[145], S. Haug[20], R. Hauser[106], L. B. Havener[39], M. Havranek[142], C. M. Hawkes[21], R. J. Hawkings[36], D. Hayden[106], C. Hayes[105], R. L. Hayes[175], C. P. Hays[135], J. M. Hays[92], H. S. Hayward[90], S. J. Haywood[144], F. He[60a], M. P. Heath[50], V. Hedberg[96], S. Heer[24], K. K. Heidegger[52], W. D. Heidorn[78], J. Heilman[34],

S. Heim[46], T. Heim[18], B. Heinemann[46,am], J. J. Heinrich[131], L. Heinrich[36], J. Hejbal[141], L. Helary[61b], A. Held[124], S. Hellesund[134], C. M. Helling[146], S. Hellman[45a,45b], C. Helsens[36], R. C. W. Henderson[89], Y. Heng[181], L. Henkelmann[61a], S. Henkelmann[175], A. M. Henriques Correia[36], H. Herde[26], V. Herget[177], Y. Hernández Jiménez[33d], H. Herr[99], M. G. Herrmann[113], T. Herrmann[48], G. Herten[52], R. Hertenberger[113], L. Hervas[36], T. C. Herwig[137], G. G. Hesketh[94], N. P. Hessey[168a], A. Higashida[163], S. Higashino[81], E. Higón-Rodriguez[174], K. Hildebrand[37], J. C. Hill[32], K. K. Hill[29], K. H. Hiller[46], S. J. Hillier[21], M. Hils[48], I. Hinchliffe[18], F. Hinterkeuser[24], M. Hirose[133], S. Hirose[52], D. Hirschbuehl[182], B. Hiti[91], O. Hladik[141], D. R. Hlaluku[33d], J. Hobbs[155], N. Hod[180], M. C. Hodgkinson[149], A. Hoecker[36], D. Hohn[52], D. Hohov[132], T. Holm[24], T. R. Holmes[37], M. Holzbock[113], L. B. A. H. Hommels[32], S. Honda[169], T. M. Hong[139], J. C. Honig[52], A. Hönle[114], B. H. Hooberman[173], W. H. Hopkins[6], Y. Horii[116], P. Horn[48], L. A. Horyn[37], S. Hou[158], A. Hoummada[35a], J. Howarth[100], J. Hoya[88], M. Hrabovsky[130], J. Hrdinka[76], I. Hristova[19], J. Hrivnac[132], A. Hrynevich[108], T. Hryn'ova[5], P. J. Hsu[64], S.-C. Hsu[148], Q. Hu[29], S. Hu[60c], Y. F. Hu[15a,15d], D. P. Huang[94], Y. Huang[60a], Y. Huang[15a], Z. Hubacek[142], F. Hubaut[101], M. Huebner[24], F. Huegging[24], T. B. Huffman[135], M. Huhtinen[36], R. F. H. Hunter[34], P. Huo[155], N. Huseynov[79,ad], J. Huston[106], J. Huth[59], R. Hyneman[105], S. Hyrych[28a], G. Iacobucci[54], G. Iakovidis[29], I. Ibragimov[151], L. Iconomidou-Fayard[132], P. Iengo[36], R. Ignazzi[40], O. Igonkina[119,z,*], R. Iguchi[163], T. Iizawa[54], Y. Ikegami[81], M. Ikeno[81], D. Iliadis[162], N. Ilic[118,167,ac], F. Iltzsche[48], G. Introzzi[70a,70b], M. Iodice[74a], K. Iordanidou[168a], V. Ippolito[72a,72b], M. F. Isacson[172], M. Ishino[163], W. Islam[129], C. Issever[19,46], S. Istin[160], F. Ito[169], J. M. Iturbe Ponce[63a], R. Iuppa[75a,75b], A. Ivina[180], H. Iwasaki[81], J. M. Izen[43], V. Izzo[69a], P. Jacka[141], P. Jackson[1], R. M. Jacobs[24], B. P. Jaeger[152], V. Jain[2], G. Jäkel[182], K. B. Jakobi[99], K. Jakobs[52], T. Jakoubek[141], J. Jamieson[57], K. W. Janas[83a], R. Jansky[54], M. Janus[53], P. A. Janus[83a], G. Jarlskog[96], N. Javadov[79,ad], T. Javůrek[36], M. Javurkova[102], F. Jeanneau[145], L. Jeanty[131], J. Jejelava[159a], A. Jelinskas[178], P. Jenni[52,b], N. Jeong[46], S. Jézéquel[5], H. Ji[181], J. Jia[155], H. Jiang[78], Y. Jiang[60a], Z. Jiang[153,p], S. Jiggins[52], F. A. Jimenez Morales[38], J. Jimenez Pena[114], S. Jin[15c], A. Jinaru[27b], O. Jinnouchi[165], H. Jivan[33d], P. Johansson[149], K. A. Johns[7], C. A. Johnson[65], R. W. L. Jones[89], S. D. Jones[156], S. Jones[7], T. J. Jones[90], J. Jongmanns[61a], P. M. Jorge[140a], J. Jovicevic[36], X. Ju[18], J. J. Junggeburth[114], A. Juste Rozas[14,x], A. Kaczmarska[84], M. Kado[72a,72b], H. Kagan[126], M. Kagan[153], A. Kahn[39], C. Kahra[99], T. Kaji[179], E. Kajomovitz[160], C. W. Kalderon[29], A. Kaluza[99], A. Kamenshchikov[122], M. Kaneda[163], N. J. Kang[146], S. Kang[78], L. Kanjir[91], Y. Kano[116], J. Kanzaki[81], L. S. Kaplan[181], D. Kar[33d], K. Karava[135], M. J. Kareem[168b], S. N. Karpov[79], Z. M. Karpova[79], V. Kartvelishvili[89], A. N. Karyukhin[122], A. Kastanas[45a,45b], C. Kato[60c,60d], J. Katzy[46], K. Kawade[150], K. Kawagoe[87], T. Kawaguchi[116], T. Kawamoto[145], G. Kawamura[53], E. F. Kay[176], V. F. Kazanin[121a,121b], R. Keeler[176], R. Kehoe[42], J. S. Keller[34], E. Kellermann[96], D. Kelsey[156], J. J. Kempster[21], J. Kendrick[21], K. E. Kennedy[39], O. Kepka[141], S. Kersten[182], B. P. Kerševan[91], S. Ketabchi Haghighat[167], M. Khader[173], F. Khalil-Zada[13], M. Khandoga[145], A. Khanov[129], A. G. Kharlamov[121a,121b], T. Kharlamova[121a,121b], E. E. Khoda[175], A. Khodinov[166], T. J. Khoo[54], E. Khramov[79], J. Khubua[159b], S. Kido[82], M. Kiehn[54], C. R. Kilby[93], E. Kim[165], Y. K. Kim[37], N. Kimura[94], O. M. Kind[19], B. T. King[90,*], D. Kirchmeier[48], J. Kirk[144], A. E. Kiryunin[114], T. Kishimoto[163], D. P. Kisliuk[167], V. Kitali[46], O. Kivernyk[5], T. Klapdor-Kleingrothaus[52], M. Klassen[61a], C. Klein[32], M. H. Klein[105], M. Klein[90], U. Klein[90], K. Kleinknecht[99], P. Klimek[120], A. Klimentov[29], T. Klingl[24], T. Klioutchnikova[36], F. F. Klitzner[113], P. Kluit[119], S. Kluth[114], E. Kneringer[76], E. B. F. G. Knoops[101], A. Knue[52], D. Kobayashi[87], T. Kobayashi[163], M. Kobel[48], M. Kocian[153], T. Kodama[163], P. Kodys[143], P. T. Koenig[24], T. Koffas[34], N. M. Köhler[36], M. Kolb[145], I. Koletsou[5], T. Komarek[130], T. Kondo[81], K. Köneke[52], A. X. Y. Kong[1], A. C. König[118], T. Kono[125], V. Konstantinides[94], N. Konstantinidis[94], B. Konya[96], R. Kopeliansky[65], S. Koperny[83a], K. Korcyl[84], K. Kordas[162], G. Koren[161], A. Korn[94], I. Korolkov[14], E. V. Korolkova[149], N. Korotkova[112], O. Kortner[114], S. Kortner[114], T. Kosek[143], V. V. Kostyukhin[149,166], A. Kotsokechagia[132], A. Kotwal[49], A. Koulouris[10], A. Kourkoumeli-Charalampidi[70a,70b], C. Kourkoumelis[9], E. Kourlitis[149], V. Kouskoura[29], A. B. Kowalewska[84], R. Kowalewski[176], W. Kozanecki[100], A. S. Kozhin[122], V. A. Kramarenko[112], G. Kramberger[91], D. Krasnopevtsev[60a], M. W. Krasny[136], A. Krasznahorkay[36], D. Krauss[114], J. A. Kremer[83a], J. Kretzschmar[90], P. Krieger[167], F. Krieter[113], A. Krishnan[61b], K. Krizka[18], K. Kroeninger[47], H. Kroha[114], J. Kroll[141], J. Kroll[137], K. S. Krowpman[106], U. Kruchonak[79], H. Krüger[24], N. Krumnack[78], M. C. Kruse[49], J. A. Krzysiak[84], T. Kubota[104], O. Kuchinskaia[166], S. Kuday[4b], J. T. Kuechler[46], S. Kuehn[36], A. Kugel[61a], T. Kuhl[46], V. Kukhtin[79], R. Kukla[101], Y. Kulchitsky[107,af], S. Kuleshov[147c], Y. P. Kulinich[173], M. Kuna[58], T. Kunigo[85], A. Kupco[141], T. Kupfer[47], O. Kuprash[52], H. Kurashige[82], L. L. Kurchaninov[168a], Y. A. Kurochkin[107], A. Kurova[111], M. G. Kurth[15a,15d], E. S. Kuwertz[36], M. Kuze[165], A. K. Kvam[148], J. Kvita[130], T. Kwan[103], L. La Rotonda[41a,41b], F. La Ruffa[41a,41b], C. Lacasta[174], F. Lacava[72a,72b], D. P. J. Lack[100], H. Lacker[19], D. Lacour[136], E. Ladygin[79], R. Lafaye[5], B. Laforge[136], T. Lagouri[147b], S. Lai[53], I. K. Lakomiec[83a], S. Lammers[65], W. Lampl[7], C. Lampoudis[162], E. Lançon[29], U. Landgraf[52], M. P. J. Landon[92], M. C. Lanfermann[54], V. S. Lang[46], J. C. Lange[53], R. J. Langenberg[102], A. J. Lankford[171], F. Lanni[29], K. Lantzsch[24], A. Lanza[70a], A. Lapertosa[55a,55b], S. Laplace[136], J. F. Laporte[145], T. Lari[68a], F. Lasagni Manghi[23a,23b], M. Lassnig[36], T. S. Lau[63a], A. Laudrain[132], A. Laurier[34], M. Lavorgna[69a,69b], S. D. Lawlor[93], M. Lazzaroni[68a,68b],

B. Le[104], E. Le Guirriec[101], A. Lebedev[78], M. LeBlanc[7], T. LeCompte[6], F. Ledroit-Guillon[58], A. C. A. Lee[94], C. A. Lee[29], G. R. Lee[17], L. Lee[59], S. C. Lee[158], S. Lee[78], B. Lefebvre[168a], H. P. Lefebvre[93], M. Lefebvre[176], C. Leggett[18], K. Lehmann[152], N. Lehmann[182], G. Lehmann Miotto[36], W. A. Leight[46], A. Leisos[162,w], M. A. L. Leite[80d], C. E. Leitgeb[113], R. Leitner[143], D. Lellouch[180,*], K. J. C. Leney[42], T. Lenz[24], R. Leone[7], S. Leone[71a], C. Leonidopoulos[50], A. Leopold[136], C. Leroy[109], R. Les[167], C. G. Lester[32], M. Levchenko[138], J. Levêque[5], D. Levin[105], L. J. Levinson[180], D. J. Lewis[21], B. Li[15b], B. Li[105], C.-Q. Li[60a], F. Li[60c], H. Li[60a], H. Li[60b], J. Li[60c], K. Li[148], L. Li[60c], M. Li[15a,15d], Q. Li[15a,15d], Q. Y. Li[60a], S. Li[60c,60d], X. Li[46], Y. Li[46], Z. Li[60b], Z. Li[103], Z. Liang[15a], B. Liberti[73a], A. Liblong[167], K. Lie[63c], S. Lim[29], C. Y. Lin[32], K. Lin[106], T. H. Lin[99], R. A. Linck[65], J. H. Lindon[21], A. L. Lionti[54], E. Lipeles[137], A. Lipniacka[17], T. M. Liss[173,an], A. Lister[175], J. D. Little[8], B. Liu[78], B. L. Liu[6], H. B. Liu[29], H. Liu[105], J. B. Liu[60a], J. K. K. Liu[37], K. Liu[60d], M. Liu[60a], P. Liu[15a], Y. Liu[15a,15d], Y. L. Liu[105], Y. W. Liu[60a], M. Livan[70a,70b], A. Lleres[58], J. Llorente Merino[152], S. L. Lloyd[92], C. Y. Lo[63b], E. M. Lobodzinska[46], P. Loch[7], S. Loffredo[73a,73b], T. Lohse[19], K. Lohwasser[149], M. Lokajicek[141], J. D. Long[173], R. E. Long[89], L. Longo[36], K. A. Looper[126], J. A. Lopez[147c], I. Lopez Paz[100], A. Lopez Solis[149], J. Lorenz[113], N. Lorenzo Martinez[5], A. M. Lory[113], M. Losada[22], P. J. Lösel[113], A. Lösle[52], X. Lou[46], X. Lou[15a], A. Lounis[132], J. Love[6], P. A. Love[89], J. J. Lozano Bahilo[174], M. Lu[60a], Y. J. Lu[64], H. J. Lubatti[148], C. Luci[72a,72b], A. Lucotte[58], C. Luedtke[52], F. Luehring[65], I. Luise[136], L. Luminari[72a], B. Lund-Jensen[154], M. S. Lutz[102], D. Lynn[29], H. Lyons[90], R. Lysak[141], E. Lytken[96], F. Lyu[15a], V. Lyubushkin[79], T. Lyubushkina[79], H. Ma[29], L. L. Ma[60b], Y. Ma[60b], G. Maccarrone[51], A. Macchiolo[114], C. M. Macdonald[149], J. Machado Miguens[137], D. Madaffari[174], R. Madar[38], W. F. Mader[48], M. Madugoda Ralalage Don[129], N. Madysa[48], J. Maeda[82], T. Maeno[29], M. Maerker[48], V. Magerl[52], N. Magini[78], D. J. Mahon[39], C. Maidantchik[80b], T. Maier[113], A. Maio[140a,140b,140d], K. Maj[83a], O. Majersky[28a], S. Majewski[131], Y. Makida[81], N. Makovec[132], B. Malaescu[136], Pa. Malecki[84], V. P. Maleev[138], F. Malek[58], U. Mallik[77], D. Malon[6], C. Malone[32], S. Maltezos[10], S. Malyukov[79], J. Mamuzic[174], G. Mancini[51], I. Mandić[91], L. Manhaes de Andrade Filho[80a], I. M. Maniatis[162], J. Manjarres Ramos[48], K. H. Mankinen[96], A. Mann[113], A. Manousos[76], B. Mansoulie[145], I. Manthos[162], S. Manzoni[119], A. Marantis[162], G. Marceca[30], L. Marchese[135], G. Marchiori[136], M. Marcisovsky[141], L. Marcoccia[73a,73b], C. Marcon[96], C. A. Marin Tobon[36], M. Marjanovic[128], Z. Marshall[18], M. U. F. Martensson[172], S. Marti-Garcia[174], C. B. Martin[126], T. A. Martin[178], V. J. Martin[50], B. Martin dit Latour[17], L. Martinelli[74a,74b], M. Martinez[14,x], V. I. Martinez Outschoorn[102], S. Martin-Haugh[144], V. S. Martoiu[27b], A. C. Martyniuk[94], A. Marzin[36], S. R. Maschek[114], L. Masetti[99], T. Mashimo[163], R. Mashinistov[110], J. Masik[100], A. L. Maslennikov[121a,121b], L. Massa[73a,73b], P. Massarotti[69a,69b], P. Mastrandrea[71a,71b], A. Mastroberardino[41a,41b], T. Masubuchi[163], D. Matakias[29], A. Matic[113], N. Matsuzawa[163], P. Mättig[24], J. Maurer[27b], B. Maček[91], D. A. Maximov[121a,121b], R. Mazini[158], I. Maznas[162], S. M. Mazza[146], S. P. Mc Kee[105], T. G. McCarthy[114], W. P. McCormack[18], E. F. McDonald[104], J. A. Mcfayden[36], G. Mchedlidze[159b], M. A. McKay[42], K. D. McLean[176], S. J. McMahon[144], P. C. McNamara[104], C. J. McNicol[178], R. A. McPherson[176,ac], J. E. Mdhluli[33d], Z. A. Meadows[102], S. Meehan[36], T. Megy[52], S. Mehlhase[113], A. Mehta[90], T. Meideck[58], B. Meirose[43], D. Melini[160], B. R. Mellado Garcia[33d], J. D. Mellenthin[53], M. Melo[28a], F. Meloni[46], A. Melzer[24], S. B. Menary[100], E. D. Mendes Gouveia[140a,140e], L. Meng[36], X. T. Meng[105], S. Menke[114], E. Meoni[41a,41b], S. Mergelmeyer[19], S. A. M. Merkt[139], C. Merlassino[135], P. Mermod[54], L. Merola[69a,69b], C. Meroni[68a], G. Merz[105], O. Meshkov[112,110], J. K. R. Meshreki[151], A. Messina[72a,72b], J. Metcalfe[6], A. S. Mete[6], C. Meyer[65], J.-P. Meyer[145], H. Meyer Zu Theenhausen[61a], F. Miano[156], M. Michetti[19], R. P. Middleton[144], L. Mijović[50], G. Mikenberg[180], M. Mikestikova[141], M. Mikuž[91], H. Mildner[149], M. Milesi[104], A. Milic[167], D. A. Millar[92], D. W. Miller[37], A. Milov[180], D. A. Milstead[45a,45b], R. A. Mina[153], A. A. Minaenko[122], M. Miñano Moya[174], I. A. Minashvili[159b], A. I. Mincer[124], B. Mindur[83a], M. Mineev[79], Y. Minegishi[163], L. M. Mir[14], A. Mirto[67a,67b], K. P. Mistry[137], T. Mitani[179], J. Mitrevski[113], V. A. Mitsou[174], M. Mittal[60c], O. Miu[167], A. Miucci[20], P. S. Miyagawa[149], A. Mizukami[81], J. U. Mjörnmark[96], T. Mkrtchyan[61a], M. Mlynarikova[143], T. Moa[45a,45b], K. Mochizuki[109], P. Mogg[52], S. Mohapatra[39], R. Moles-Valls[24], M. C. Mondragon[106], K. Mönig[46], J. Monk[40], E. Monnier[101], A. Montalbano[152], J. Montejo Berlingen[36], M. Montella[94], F. Monticelli[88], S. Monzani[68a], N. Morange[132], D. Moreno[22], M. Moreno Llácer[174], C. Moreno Martinez[14], P. Morettini[55b], M. Morgenstern[160], S. Morgenstern[48], D. Mori[152], M. Morii[59], M. Morinaga[179], V. Morisbak[134], A. K. Morley[36], G. Mornacchi[36], A. P. Morris[94], L. Morvaj[155], P. Moschovakos[36], B. Moser[119], M. Mosidze[159b], T. Moskalets[145], H. J. Moss[149], J. Moss[31,m], E. J. W. Moyse[102], S. Muanza[101], J. Mueller[139], R. S. P. Mueller[113], D. Muenstermann[89], G. A. Mullier[96], D. P. Mungo[68a,68b], J. L. Munoz Martinez[14], F. J. Munoz Sanchez[100], P. Murin[28b], W. J. Murray[144,178], A. Murrone[68a,68b], M. Muškinja[18], C. Mwewa[33a], A. G. Myagkov[122,ai], A. A. Myers[139], J. Myers[131], M. Myska[142], B. P. Nachman[18], O. Nackenhorst[47], A.Nag Nag[48], K. Nagai[135], K. Nagano[81], Y. Nagasaka[62], J. L. Nagle[29], E. Nagy[101], A. M. Nairz[36], Y. Nakahama[116], K. Nakamura[81], T. Nakamura[163], I. Nakano[127], H. Nanjo[133], F. Napolitano[61a], R. F. Naranjo Garcia[46], R. Narayan[42], I. Naryshkin[138], T. Naumann[46], G. Navarro[22], P. Y. Nechaeva[110], F. Nechansky[46], T. J. Neep[21], A. Negri[70a,70b], M. Negrini[23b], C. Nellist[118], M. E. Nelson[45a,45b], S. Nemecek[141], M. Nessi[36,d],

M. S. Neubauer[173], F. Neuhaus[99], M. Neumann[182], R. Newhouse[175], P. R. Newman[21], C. W. Ng[139], Y. S. Ng[19], Y. W. Y. Ng[171], B. Ngair[35e], H. D. N. Nguyen[101], T. Nguyen Manh[109], E. Nibigira[38], R. B. Nickerson[135], R. Nicolaidou[145], D. S. Nielsen[40], J. Nielsen[146], N. Nikiforou[11], V. Nikolaenko[122,ai], I. Nikolic-Audit[136], K. Nikolopoulos[21], P. Nilsson[29], H. R. Nindhito[54], Y. Ninomiya[81], A. Nisati[72a], N. Nishu[60c], R. Nisius[114], I. Nitsche[47], T. Nitta[179], T. Nobe[163], Y. Noguchi[85], I. Nomidis[136], M. A. Nomura[29], M. Nordberg[36], T. Novak[91], O. Novgorodova[48], R. Novotny[142], L. Nozka[130], K. Ntekas[171], E. Nurse[94], F. G. Oakham[34,ap], H. Oberlack[114], J. Ocariz[136], A. Ochi[82], I. Ochoa[39], J. P. Ochoa-Ricoux[147a], K. O'Connor[26], S. Oda[87], S. Odaka[81], S. Oerdek[53], A. Ogrodnik[83a], A. Oh[100], S. H. Oh[49], C. C. Ohm[154], H. Oide[165], M. L. Ojeda[167], H. Okawa[169], Y. Okazaki[85], M. W. O'Keefe[90], Y. Okumura[163], T. Okuyama[81], A. Olariu[27b], L. F. Oleiro Seabra[140a], S. A. Olivares Pino[147a], D. Oliveira Damazio[29], J. L. Oliver[1], M. J. R. Olsson[171], A. Olszewski[84], J. Olszowska[84], D. C. O'Neil[152], A. P. O'neill[135], A. Onofre[140a,140e], P. U. E. Onyisi[11], H. Oppen[134], M. J. Oreglia[37], G. E. Orellana[88], D. Orestano[74a,74b], N. Orlando[14], R. S. Orr[167], V. O'Shea[57], R. Ospanov[60a], G. Otero y Garzon[30], H. Otono[87], P. S. Ott[61a], M. Ouchrif[35d], J. Ouellette[29], F. Ould-Saada[134], A. Ouraou[145], Q. Ouyang[15a], M. Owen[57], R. E. Owen[21], V. E. Ozcan[12c], N. Ozturk[8], J. Pacalt[130], H. A. Pacey[32], K. Pachal[49], A. Pacheco Pages[14], C. Padilla Aranda[14], S. Pagan Griso[18], M. Paganini[183], G. Palacino[65], S. Palazzo[50], S. Palestini[36], M. Palka[83b], D. Pallin[38], P. Palni[83a], I. Panagoulias[10], C. E. Pandini[36], J. G. Panduro Vazquez[93], P. Pani[46], G. Panizzo[66a,66c], L. Paolozzi[54], C. Papadatos[109], K. Papageorgiou[9,g], S. Parajuli[42], A. Paramonov[6], D. Paredes Hernandez[63b], S. R. Paredes Saenz[135], B. Parida[166], T. H. Park[167], A. J. Parker[31], M. A. Parker[32], F. Parodi[55a,55b], E. W. Parrish[120], J. A. Parsons[39], U. Parzefall[52], L. Pascual Dominguez[136], V. R. Pascuzzi[167], J. M. P. Pasner[146], F. Pasquali[119], E. Pasqualucci[72a], S. Passaggio[55b], F. Pastore[93], P. Pasuwan[45a,45b], S. Pataraia[99], J. R. Pater[100], A. Pathak[181,i], J. Patton[90], T. Pauly[36], J. Pearkes[153], B. Pearson[114], M. Pedersen[134], L. Pedraza Diaz[118], R. Pedro[140a], T. Peiffer[53], S. V. Peleganchuk[121a,121b], O. Penc[141], H. Peng[60a], B. S. Peralva[80a], M. M. Perego[132], A. P. Pereira Peixoto[140a], D. V. Perepelitsa[29], F. Peri[19], L. Perini[68a,68b], H. Pernegger[36], S. Perrella[140a], A. Perrevoort[119], K. Peters[46], R. F. Y. Peters[100], B. A. Petersen[36], T. C. Petersen[40], E. Petit[101], A. Petridis[1], C. Petridou[162], P. Petroff[132], M. Petrov[135], F. Petrucci[74a,74b], M. Pettee[183], N. E. Pettersson[102], K. Petukhova[143], A. Peyaud[145], R. Pezoa[147c], L. Pezzotti[70a,70b], T. Pham[104], F. H. Phillips[106], P. W. Phillips[144], M. W. Phipps[173], G. Piacquadio[155], E. Pianori[18], A. Picazio[102], R. H. Pickles[100], R. Piegaia[30], D. Pietreanu[27b], J. E. Pilcher[37], A. D. Pilkington[100], M. Pinamonti[66a,66c], J. L. Pinfold[3], M. Pitt[161], L. Pizzimento[73a,73b], M.-A. Pleier[29], V. Pleskot[143], E. Plotnikova[79], P. Podberezko[121a,121b], R. Poettgen[96], R. Poggi[54], L. Poggioli[136], I. Pogrebnyak[106], D. Pohl[24], I. Pokharel[53], G. Polesello[70a], A. Poley[18], A. Policicchio[72a,72b], R. Polifka[143], A. Polini[23b], C. S. Pollard[46], V. Polychronakos[29], D. Ponomarenko[111], L. Pontecorvo[36], S. Popa[27a], G. A. Popeneciu[27d], L. Portales[5], D. M. Portillo Quintero[58], S. Pospisil[142], K. Potamianos[46], I. N. Potrap[79], C. J. Potter[32], H. Potti[11], T. Poulsen[96], J. Poveda[36], T. D. Powell[149], G. Pownall[46], M. E. Pozo Astigarraga[36], P. Pralavorio[101], S. Prell[78], D. Price[100], M. Primavera[67a], S. Prince[103], M. L. Proffitt[148], N. Proklova[111], K. Prokofiev[63c], F. Prokoshin[79], S. Protopopescu[29], J. Proudfoot[6], M. Przybycien[83a], D. Pudzha[138], A. Puri[173], P. Puzo[132], J. Qian[105], Y. Qin[100], A. Quadt[53], M. Queitsch-Maitland[36], A. Qureshi[1], M. Racko[28a], F. Ragusa[68a,68b], G. Rahal[97], J. A. Raine[54], S. Rajagopalan[29], A. Ramirez Morales[92], K. Ran[15a,15d], T. Rashid[132], S. Raspopov[5], D. M. Rauch[46], F. Rauscher[113], S. Rave[99], B. Ravina[149], I. Ravinovich[180], J. H. Rawling[100], M. Raymond[36], A. L. Read[134], N. P. Readioff[58], M. Reale[67a,67b], D. M. Rebuzzi[70a,70b], A. Redelbach[177], G. Redlinger[29], K. Reeves[43], L. Rehnisch[19], J. Reichert[137], D. Reikher[161], A. Reiss[99], A. Rej[151], C. Rembser[36], A. Renardi[46], M. Renda[27b], M. Rescigno[72a], S. Resconi[68a], E. D. Resseguie[18], S. Rettie[94], B. Reynolds[126], E. Reynolds[21], O. L. Rezanova[121a,121b], P. Reznicek[143], E. Ricci[75a,75b], R. Richter[114], S. Richter[46], E. Richter-Was[83b], O. Ricken[24], M. Ridel[136], P. Rieck[114], O. Rifki[46], M. Rijssenbeek[155], A. Rimoldi[70a,70b], M. Rimoldi[46], L. Rinaldi[23b], G. Ripellino[154], I. Riu[14], J. C. Rivera Vergara[176], F. Rizatdinova[129], E. Rizvi[92], C. Rizzi[36], R. T. Roberts[100], S. H. Robertson[103,ac], M. Robin[46], D. Robinson[32], C. M. Robles Gajardo[147c], M. Robles Manzano[99], A. Robson[57], A. Rocchi[73a,73b], E. Rocco[99], C. Roda[71a,71b], S. Rodriguez Bosca[174], A. Rodriguez Perez[14], D. Rodriguez Rodriguez[174], A. M. Rodríguez Vera[168b], S. Roe[36], O. Røhne[134], R. Röhrig[114], R. A. Rojas[147c], B. Roland[52], C. P. A. Roland[65], J. Roloff[29], A. Romaniouk[111], M. Romano[23a,23b], N. Rompotis[90], M. Ronzani[124], L. Roos[136], S. Rosati[72a], G. Rosin[102], B. J. Rosser[137], E. Rossi[46], E. Rossi[74a,74b], E. Rossi[69a,69b], L. P. Rossi[55b], L. Rossini[68a,68b], R. Rosten[14], M. Rotaru[27b], J. Rothberg[148], B. Rottler[52], D. Rousseau[132], G. Rovelli[70a,70b], A. Roy[11], D. Roy[33d], A. Rozanov[101], Y. Rozen[160], X. Ruan[33d], F. Rühr[52], A. Ruiz-Martinez[174], A. Rummler[36], Z. Rurikova[52], N. A. Rusakovich[79], H. L. Russell[103], L. Rustige[38,47], J. P. Rutherfoord[7], E. M. Rüttinger[149], M. Rybar[39], G. Rybkin[132], E. B. Rye[134], A. Ryzhov[122], J. A. Sabater Iglesias[46], P. Sabatini[53], G. Sabato[119], S. Sacerdoti[132], H.F-W. Sadrozinski[146], R. Sadykov[79], F. Safai Tehrani[72a], B. Safarzadeh Samani[156], M. Safdari[153], P. Saha[120], S. Saha[103], M. Sahinsoy[61a], A. Sahu[182], M. Saimpert[46], M. Saito[163], T. Saito[163], H. Sakamoto[163], D. Salamani[54], G. Salamanna[74a,74b], J. E. Salazar Loyola[147c], A. Salnikov[153], J. Salt[174], D. Salvatore[41a,41b], F. Salvatore[156], A. Salvucci[63a,63b,63c], A. Salzburger[36], J. Samarati[36], D. Sammel[52], D. Sampsonidis[162], D. Sampsonidou[162],

J. Sánchez[174], A. Sanchez Pineda[36,66a,66c], H. Sandaker[134], C. O. Sander[46], I. G. Sanderswood[89], M. Sandhoff[182], C. Sandoval[22], D. P. C. Sankey[144], M. Sannino[55a,55b], Y. Sano[116], A. Sansoni[51], C. Santoni[38], H. Santos[140a,140b], S. N. Santpur[18], A. Santra[174], A. Sapronov[79], J. G. Saraiva[140a,140d], O. Sasaki[81], K. Sato[169], F. Sauerburger[52], E. Sauvan[5], P. Savard[167,ap], R. Sawada[163], C. Sawyer[144], L. Sawyer[95,ah], C. Sbarra[23b], A. Sbrizzi[23a], T. Scanlon[94], J. Schaarschmidt[148], P. Schacht[114], B. M. Schachtner[113], D. Schaefer[37], L. Schaefer[137], J. Schaeffer[99], S. Schaepe[36], U. Schäfer[99], A. C. Schaffer[132], D. Schaile[113], R. D. Schamberger[155], N. Scharmberg[100], V. A. Schegelsky[138], D. Scheirich[143], F. Schenck[19], M. Schernau[171], C. Schiavi[55a,55b], L. K. Schildgen[24], Z. M. Schillaci[26], E. J. Schioppa[36], M. Schioppa[41a,41b], K. E. Schleicher[52], S. Schlenker[36], K. R. Schmidt-Sommerfeld[114], K. Schmieden[36], C. Schmitt[99], S. Schmitt[46], S. Schmitz[99], J. C. Schmoeckel[46], L. Schoeffel[145], A. Schoening[61b], P. G. Scholer[52], E. Schopf[135], M. Schott[99], J. F. P. Schouwenberg[118], J. Schovancova[36], S. Schramm[54], F. Schroeder[182], A. Schulte[99], H.-C. Schultz-Coulon[61a], M. Schumacher[52], B. A. Schumm[146], Ph. Schune[145], A. Schwartzman[153], T. A. Schwarz[105], Ph. Schwemling[145], R. Schwienhorst[106], A. Sciandra[146], G. Sciolla[26], M. Scodeggio[46], M. Scornajenghi[41a,41b], F. Scuri[71a], F. Scutti[104], L. M. Scyboz[114], C. D. Sebastiani[72a,72b], P. Seema[19], S. C. Seidel[117], A. Seiden[146], B. D. Seidlitz[29], T. Seiss[37], J. M. Seixas[80b], G. Sekhniaidze[69a], S. J. Sekula[42], N. Semprini-Cesari[23a,23b], S. Sen[49], C. Serfon[76], L. Serin[132], L. Serkin[66a,66b], M. Sessa[60a], H. Severini[128], S. Sevova[153], T. Šfiligoj[91], F. Sforza[55a,55b], A. Sfyrla[54], E. Shabalina[53], J. D. Shahinian[146], N. W. Shaikh[45a,45b], D. Shaked Renous[180], L. Y. Shan[15a], M. Shapiro[18], A. Sharma[135], A. S. Sharma[1], P. B. Shatalov[123], K. Shaw[156], S. M. Shaw[100], M. Shehade[180], Y. Shen[128], A. D. Sherman[25], P. Sherwood[94], L. Shi[158], S. Shimizu[81], C. O. Shimmin[183], Y. Shimogama[179], M. Shimojima[115], I. P. J. Shipsey[135], S. Shirabe[165], M. Shiyakova[79,aa], J. Shlomi[180], A. Shmeleva[110], M. J. Shochet[37], J. Shojaii[104], D. R. Shope[128], S. Shrestha[126], E. M. Shrif[33d], E. Shulga[180], P. Sicho[141], A. M. Sickles[173], P. E. Sidebo[154], E. Sideras Haddad[33d], O. Sidiropoulou[36], A. Sidoti[23a,23b], F. Siegert[48], Dj. Sijacki[16], M. Jr. Silva[181], M. V. Silva Oliveira[80a], S. B. Silverstein[45a], S. Simion[132], R. Simoniello[99], S. Simsek[12b], P. Sinervo[167], V. Sinetckii[112], S. Singh[152], M. Sioli[23a,23b], I. Siral[131], S. Yu. Sivoklokov[112], J. Sjölin[45a,45b], E. Skorda[96], P. Skubic[128], M. Slawinska[84], K. Sliwa[170], R. Slovak[143], V. Smakhtin[180], B. H. Smart[144], J. Smiesko[28b], N. Smirnov[111], S. Yu. Smirnov[111], Y. Smirnov[111], L. N. Smirnova[112,t], O. Smirnova[96], J. W. Smith[53], M. Smizanska[89], K. Smolek[142], A. Smykiewicz[84], A. A. Snesarev[110], H. L. Snoek[119], I. M. Snyder[131], S. Snyder[29], R. Sobie[176,ac], A. Soffer[161], A. Søgaard[50], F. Sohns[53], C. A. Solans Sanchez[36], E. Yu. Soldatov[111], U. Soldevila[174], A. A. Solodkov[122], A. Soloshenko[79], O. V. Solovyanov[122], V. Solovyev[138], P. Sommer[149], H. Son[170], W. Song[144], W. Y. Song[168b], A. Sopczak[142], A. L. Sopio[94], F. Sopkova[28b], C. L. Sotiropoulou[71a,71b], S. Sottocornola[70a,70b], R. Soualah[66a,66c,f], A. M. Soukharev[121a,121b], D. South[46], S. Spagnolo[67a,67b], M. Spalla[114], M. Spangenberg[178], F. Spanò[93], D. Sperlich[52], T. M. Spieker[61a], G. Spigo[36], M. Spina[156], D. P. Spiteri[57], M. Spousta[143], A. Stabile[68a,68b], B. L. Stamas[120], R. Stamen[61a], M. Stamenkovic[119], E. Stanecka[84], B. Stanislaus[135], M. M. Stanitzki[46], M. Stankaityte[135], B. Stapf[119], E. A. Starchenko[122], G. H. Stark[146], J. Stark[58], P. Staroba[141], P. Starovoitov[61a], S. Stärz[103], R. Staszewski[84], G. Stavropoulos[44], M. Stegler[46], P. Steinberg[29], A. L. Steinhebel[131], B. Stelzer[152], H. J. Stelzer[139], O. Stelzer-Chilton[168a], H. Stenzel[56], T. J. Stevenson[156], G. A. Stewart[36], M. C. Stockton[36], G. Stoicea[27b], M. Stolarski[140a], S. Stonjek[114], A. Straessner[48], J. Strandberg[154], S. Strandberg[45a,45b], M. Strauss[128], P. Strizenec[28b], R. Ströhmer[177], D. M. Strom[131], R. Stroynowski[42], A. Strubig[50], S. A. Stucci[29], B. Stugu[17], J. Stupak[128], N. A. Styles[46], D. Su[153], W. Su[60c], S. Suchek[61a], V. V. Sulin[110], M. J. Sullivan[90], D. M. S. Sultan[54], S. Sultansoy[4c], T. Sumida[85], S. Sun[105], X. Sun[100], K. Suruliz[156], C. J. E. Suster[157], M. R. Sutton[156], S. Suzuki[81], M. Svatos[141], M. Swiatlowski[37], S. P. Swift[2], T. Swirski[177], A. Sydorenko[99], I. Sykora[28a], M. Sykora[143], T. Sykora[143], D. Ta[99], K. Tackmann[46,y], J. Taenzer[161], A. Taffard[171], R. Tafirout[168a], R. Takashima[86], K. Takeda[82], T. Takeshita[150], E. P. Takeva[50], Y. Takubo[81], M. Talby[101], A. A. Talyshev[121a,121b], N. M. Tamir[161], J. Tanaka[163], M. Tanaka[165], R. Tanaka[132], S. Tapia Araya[173], S. Tapprogge[99], A. Tarek Abouelfadl Mohamed[136], S. Tarem[160], K. Tariq[60b], G. Tarna[27b,c], G. F. Tartarelli[68a], P. Tas[143], M. Tasevsky[141], T. Tashiro[85], E. Tassi[41a,41b], A. Tavares Delgado[140a], Y. Tayalati[35e], A. J. Taylor[50], G. N. Taylor[104], W. Taylor[168b], A. S. Tee[89], R. Teixeira De Lima[153], P. Teixeira-Dias[93], H. Ten Kate[36], J. J. Teoh[119], S. Terada[81], K. Terashi[163], J. Terron[98], S. Terzo[14], M. Testa[51], R. J. Teuscher[167,ac], S. J. Thais[183], T. Theveneaux-Pelzer[46], F. Thiele[40], D. W. Thomas[93], J. O. Thomas[42], J. P. Thomas[21], P. D. Thompson[21], L. A. Thomsen[183], E. Thomson[137], E. J. Thorpe[92], R. E. Ticse Torres[53], V. O. Tikhomirov[110,aj], Yu. A. Tikhonov[121a,121b], S. Timoshenko[111], P. Tipton[183], S. Tisserant[101], K. Todome[23a,23b], S. Todorova-Nova[143], S. Todt[48], J. Tojo[87], S. Tokár[28a], K. Tokushuku[81], E. Tolley[126], K. G. Tomiwa[33d], M. Tomoto[116], L. Tompkins[153,p], B. Tong[59], P. Tornambe[102], E. Torrence[131], H. Torres[48], E. Torró Pastor[148], C. Tosciri[135], J. Toth[101,ab], D. R. Tovey[149], A. Traeet[17], C. J. Treado[124], T. Trefzger[177], F. Tresoldi[156], A. Tricoli[29], I. M. Trigger[168a], S. Trincaz-Duvoid[136], D. T. Trischuk[175], W. Trischuk[167], B. Trocmé[58], A. Trofymov[145], C. Troncon[68a], F. Trovato[156], L. Truong[33b], M. Trzebinski[84], A. Trzupek[84], F. Tsai[46], J.C.-L. Tseng[135], P. V. Tsiareshka[107,af], A. Tsirigotis[162,w], V. Tsiskaridze[155], E. G. Tskhadadze[159a], M. Tsopoulou[162], I. I. Tsukerman[123], V. Tsulaia[18], S. Tsuno[81], D. Tsybychev[155], Y. Tu[63b], A. Tudorache[27b],

V. Tudorache[27b], T. T. Tulbure[27a], A. N. Tuna[59], S. Turchikhin[79], D. Turgeman[180], I. Turk Cakir[4b,u], R. J. Turner[21], R. T. Turra[68a], P. M. Tuts[39], S. Tzamarias[162], E. Tzovara[99], G. Ucchielli[47], K. Uchida[163], F. Ukegawa[169], G. Unal[36], A. Undrus[29], G. Unel[171], F. C. Ungaro[104], Y. Unno[81], K. Uno[163], J. Urban[28b], P. Urquijo[104], G. Usai[8], Z. Uysal[12d], V. Vacek[142], B. Vachon[103], K. O. H. Vadla[134], A. Vaidya[94], C. Valderanis[113], E. Valdes Santurio[45a,45b], M. Valente[54], S. Valentinetti[23a,23b], A. Valero[174], L. Valéry[46], R. A. Vallance[21], A. Vallier[36], J. A. Valls Ferrer[174], T. R. Van Daalen[14], P. Van Gemmeren[6], I. Van Vulpen[119], M. Vanadia[73a,73b], W. Vandelli[36], M. Vandenbroucke[145], E. R. Vandewall[129], A. Vaniachine[166], D. Vannicola[72a,72b], R. Vari[72a], E. W. Varnes[7], C. Varni[55a,55b], T. Varol[158], D. Varouchas[132], K. E. Varvell[157], M. E. Vasile[27b], G. A. Vasquez[176], F. Vazeille[38], D. Vazquez Furelos[14], T. Vazquez Schroeder[36], J. Veatch[53], V. Vecchio[74a,74b], M. J. Veen[119], L. M. Veloce[167], F. Veloso[140a,140c], S. Veneziano[72a], A. Ventura[67a,67b], N. Venturi[36], A. Verbytskyi[114], V. Vercesi[70a], M. Verducci[71a,71b], C. M. Vergel Infante[78], C. Vergis[24], W. Verkerke[119], A. T. Vermeulen[119], J. C. Vermeulen[119], M. C. Vetterli[152,ap], N. Viaux Maira[147c], M. Vicente Barreto Pinto[54], T. Vickey[149], O. E. Vickey Boeriu[149], G. H. A. Viehhauser[135], L. Vigani[61b], M. Villa[23a,23b], M. Villaplana Perez[3], E. Vilucchi[51], M. G. Vincter[34], G. S. Virdee[21], A. Vishwakarma[46], C. Vittori[23a,23b], I. Vivarelli[156], M. Vogel[182], P. Vokac[142], S. E. von Buddenbrock[33d], E. Von Toerne[24], V. Vorobel[143], K. Vorobev[111], M. Vos[174], J. H. Vossebeld[90], M. Vozak[100], N. Vranjes[16], M. Vranjes Milosavljevic[16], V. Vrba[142], M. Vreeswijk[119], R. Vuillermet[36], I. Vukotic[37], P. Wagner[24], W. Wagner[182], J. Wagner-Kuhr[113], S. Wahdan[182], H. Wahlberg[88], V. M. Walbrecht[114], J. Walder[89], R. Walker[113], S. D. Walker[93], W. Walkowiak[151], V. Wallangen[45a,45b], A. M. Wang[59], A. Z. Wang[181], C. Wang[60c], F. Wang[181], H. Wang[18], H. Wang[3], J. Wang[63a], J. Wang[61b], P. Wang[42], Q. Wang[128], R.-J. Wang[99], R. Wang[60a], R. Wang[6], S. M. Wang[158], W. T. Wang[60a], W. Wang[15c], W. X. Wang[60a], Y. Wang[60a], Z. Wang[60c], C. Wanotayaroj[46], A. Warburton[103], C. P. Ward[32], D. R. Wardrope[94], N. Warrack[57], A. Washbrook[50], A. T. Watson[21], M. F. Watson[21], G. Watts[148], B. M. Waugh[94], A. F. Webb[11], S. Webb[99], C. Weber[183], M. S. Weber[20], S. A. Weber[34], S. M. Weber[61a], A. R. Weidberg[135], J. Weingarten[47], M. Weirich[99], C. Weiser[52], P. S. Wells[36], T. Wenaus[29], T. Wengler[36], S. Wenig[36], N. Wermes[24], M. D. Werner[78], M. Wessels[61a], T. D. Weston[20], K. Whalen[131], N. L. Whallon[148], A. M. Wharton[89], A. S. White[105], A. White[8], M. J. White[1], D. Whiteson[171], B. W. Whitmore[89], W. Wiedenmann[181], C. Wiel[48], M. Wielers[144], N. Wieseotte[99], C. Wiglesworth[40], L. A. M. Wiik-Fuchs[52], H. G. Wilkens[36], L. J. Wilkins[93], H. H. Williams[137], S. Williams[32], C. Willis[106], S. Willocq[102], I. Wingerter-Seez[5], E. Winkels[156], F. Winklmeier[131], O. J. Winston[156], B. T. Winter[52], M. Wittgen[153], M. Wobisch[95], A. Wolf[99], T. M. H. Wolf[119], R. Wolff[101], R. W. Wölker[135], J. Wollrath[52], M. W. Wolter[84], H. Wolters[140a,140c], V. W. S. Wong[175], N. L. Woods[146], S. D. Worm[46], B. K. Wosiek[84], K. W. Woźniak[84], K. Wraight[57], S. L. Wu[181], X. Wu[54], Y. Wu[60a], T. R. Wyatt[100], B. M. Wynne[50], S. Xella[40], Z. Xi[105], L. Xia[178], X. Xiao[105], I. Xiotidis[156], D. Xu[15a], H. Xu[60a], H. Xu[60a], L. Xu[29], T. Xu[145], W. Xu[105], Z. Xu[60b], Z. Xu[153], B. Yabsley[157], S. Yacoob[33a], K. Yajima[133], D. P. Yallup[94], N. Yamaguchi[87], Y. Yamaguchi[165], A. Yamamoto[81], M. Yamatani[163], T. Yamazaki[163], Y. Yamazaki[82], Z. Yan[25], H. J. Yang[60c,60d], H. T. Yang[18], S. Yang[60a], T. Yang[63c], X. Yang[60b,58], Y. Yang[163], W.-M. Yao[18], Y. C. Yap[46], Y. Yasu[81], E. Yatsenko[60c,60d], H. Ye[15c], J. Ye[42], S. Ye[29], I. Yeletskikh[79], M. R. Yexley[89], E. Yigitbasi[25], K. Yorita[179], K. Yoshihara[137], C. J. S. Young[36], C. Young[153], J. Yu[78], R. Yuan[60b,h], X. Yue[61a], M. Zaazoua[35e], B. Zabinski[84], G. Zacharis[10], E. Zaffaroni[54], J. Zahreddine[136], A. M. Zaitsev[122,ai], T. Zakareishvili[159b], N. Zakharchuk[34], S. Zambito[59], D. Zanzi[36], D. R. Zaripovas[57], S. V. Zeißner[47], C. Zeitnitz[182], G. Zemaityte[135], J. C. Zeng[173], O. Zenin[122], T. Ženiš[28a], D. Zerwas[132], M. Zgubič[135], B. Zhang[15c], D. F. Zhang[15b], G. Zhang[15b], H. Zhang[15c], J. Zhang[6], L. Zhang[15c], L. Zhang[60a], M. Zhang[173], R. Zhang[181], S. Zhang[105], X. Zhang[60b], Y. Zhang[15a,15d], Z. Zhang[63a], Z. Zhang[132], P. Zhao[49], Z. Zhao[60a], A. Zhemchugov[79], Z. Zheng[105], D. Zhong[173], B. Zhou[105], C. Zhou[181], M. S. Zhou[15a,15d], M. Zhou[155], N. Zhou[60c], Y. Zhou[7], C. G. Zhu[60b], C. Zhu[15a,15d], H. L. Zhu[60a], H. Zhu[15a], J. Zhu[105], Y. Zhu[60a], X. Zhuang[15a], K. Zhukov[110], V. Zhulanov[121a,121b], D. Zieminska[65], N. I. Zimine[79], S. Zimmermann[52], Z. Zinonos[114], M. Ziolkowski[151], L. Živković[16], G. Zobernig[181], A. Zoccoli[23a,23b], K. Zoch[53], T. G. Zorbas[149], R. Zou[37], L. Zwalinski[36]

[1] Department of Physics, University of Adelaide, Adelaide, Australia
[2] Physics Department, SUNY Albany, Albany, NY, USA
[3] Department of Physics, University of Alberta, Edmonton, AB, Canada
[4] [(a)]Department of Physics, Ankara University, Ankara, Turkey; [(b)]Istanbul Aydin University, Istanbul, Turkey; [(c)]Division of Physics, TOBB University of Economics and Technology, Ankara, Turkey
[5] LAPP, Université Grenoble Alpes, Université Savoie Mont Blanc, CNRS/IN2P3, Annecy, France
[6] High Energy Physics Division, Argonne National Laboratory, Argonne, IL, USA
[7] Department of Physics, University of Arizona, Tucson, AZ, USA
[8] Department of Physics, University of Texas at Arlington, Arlington, TX, USA

[9] Physics Department, National and Kapodistrian University of Athens, Athens, Greece
[10] Physics Department, National Technical University of Athens, Zografou, Greece
[11] Department of Physics, University of Texas at Austin, Austin, TX, USA
[12] [(a)]Bahcesehir University, Faculty of Engineering and Natural Sciences, Istanbul, Turkey; [(b)]Istanbul Bilgi University, Faculty of Engineering and Natural Sciences, Istanbul, Turkey; [(c)]Department of Physics, Bogazici University, Istanbul, Turkey; [(d)]Department of Physics Engineering, Gaziantep University, Gaziantep, Turkey
[13] Institute of Physics, Azerbaijan Academy of Sciences, Baku, Azerbaijan
[14] Institut de Física d'Altes Energies (IFAE), Barcelona Institute of Science and Technology, Barcelona, Spain
[15] [(a)]Institute of High Energy Physics, Chinese Academy of Sciences, Beijing, China; [(b)]Physics Department, Tsinghua University, Beijing, China; [(c)]Department of Physics, Nanjing University, Nanjing, China; [(d)]University of Chinese Academy of Science (UCAS), Beijing, China
[16] Institute of Physics, University of Belgrade, Belgrade, Serbia
[17] Department for Physics and Technology, University of Bergen, Bergen, Norway
[18] Physics Division, Lawrence Berkeley National Laboratory and University of California, Berkeley, CA, USA
[19] Institut für Physik, Humboldt Universität zu Berlin, Berlin, Germany
[20] Albert Einstein Center for Fundamental Physics and Laboratory for High Energy Physics, University of Bern, Bern, Switzerland
[21] School of Physics and Astronomy, University of Birmingham, Birmingham, UK
[22] Facultad de Ciencias y Centro de Investigaciónes, Universidad Antonio Nariño, Bogota, Colombia
[23] [(a)]Dipartimento di Fisica, INFN Bologna and Universita' di Bologna, Bologna, Italy; [(b)]INFN Sezione di Bologna, Bologna, Italy
[24] Physikalisches Institut, Universität Bonn, Bonn, Germany
[25] Department of Physics, Boston University, Boston, MA, USA
[26] Department of Physics, Brandeis University, Waltham, MA, USA
[27] [(a)]Transilvania University of Brasov, Brasov, Romania; [(b)]Horia Hulubei National Institute of Physics and Nuclear Engineering, Bucharest, Romania; [(c)]Department of Physics, Alexandru Ioan Cuza University of Iasi, Iasi, Romania; [(d)]National Institute for Research and Development of Isotopic and Molecular Technologies, Physics Department, Cluj-Napoca, Romania; [(e)]University Politehnica Bucharest, Bucharest, Romania; [(f)]West University in Timisoara, Timisoara, Romania
[28] [(a)]Faculty of Mathematics, Physics and Informatics, Comenius University, Bratislava, Slovak Republic; [(b)]Department of Subnuclear Physics, Institute of Experimental Physics of the Slovak Academy of Sciences, Kosice, Slovak Republic
[29] Physics Department, Brookhaven National Laboratory, Upton, NY, USA
[30] Departamento de Física, Universidad de Buenos Aires, Buenos Aires, Argentina
[31] California State University, CA, USA
[32] Cavendish Laboratory, University of Cambridge, Cambridge, UK
[33] [(a)]Department of Physics, University of Cape Town, Cape Town, South Africa; [(b)]Department of Mechanical Engineering Science, University of Johannesburg, Johannesburg, South Africa; [(c)]Pretoria, South Africa; [(d)]School of Physics, University of the Witwatersrand, Johannesburg, South Africa
[34] Department of Physics, Carleton University, Ottawa, ON, Canada
[35] [(a)]Faculté des Sciences Ain Chock, Réseau Universitaire de Physique des Hautes Energies, Université Hassan II, Casablanca, Morocco; [(b)]Faculté des Sciences, Université Ibn-Tofail, Kénitra, Morocco; [(c)]Faculté des Sciences Semlalia, Université Cadi Ayyad, LPHEA-Marrakech, Marrakesh, Morocco; [(d)]Faculté des Sciences, Université Mohamed Premier and LPTPM, Oujda, Morocco; [(e)]Faculté des sciences, Université Mohammed V, Rabat, Morocco
[36] CERN, Geneva, Switzerland
[37] Enrico Fermi Institute, University of Chicago, Chicago, IL, USA
[38] LPC, Université Clermont Auvergne, CNRS/IN2P3, Clermont-Ferrand, France
[39] Nevis Laboratory, Columbia University, Irvington, NY, USA
[40] Niels Bohr Institute, University of Copenhagen, Copenhagen, Denmark
[41] [(a)]Dipartimento di Fisica, Università della Calabria, Rende, Italy; [(b)]INFN Gruppo Collegato di Cosenza, Laboratori Nazionali di Frascati, Frascati, Italy
[42] Physics Department, Southern Methodist University, Dallas, TX, USA
[43] Physics Department, University of Texas at Dallas, Richardson, TX, USA
[44] National Centre for Scientific Research "Demokritos", Agia Paraskevi, Greece

[45] [(a)]Department of Physics, Stockholm University, Stockholm, Sweden; [(b)]Oskar Klein Centre, Stockholm, Sweden
[46] Deutsches Elektronen-Synchrotron DESY, Hamburg and Zeuthen, Germany
[47] Lehrstuhl für Experimentelle Physik IV, Technische Universität Dortmund, Dortmund, Germany
[48] Institut für Kern- und Teilchenphysik, Technische Universität Dresden, Dresden, Germany
[49] Department of Physics, Duke University, Durham, NC, USA
[50] SUPA-School of Physics and Astronomy, University of Edinburgh, Edinburgh, United Kingdom
[51] INFN e Laboratori Nazionali di Frascati, Frascati, Italy
[52] Physikalisches Institut, Albert-Ludwigs-Universität Freiburg, Freiburg, Germany
[53] II. Physikalisches Institut, Georg-August-Universität Göttingen, Göttingen, Germany
[54] Département de Physique Nucléaire et Corpusculaire, Université de Genève, Geneva, Switzerland
[55] [(a)]Dipartimento di Fisica, Università di Genova, Genoa, Italy; [(b)]INFN Sezione di Genova, Genoa, Italy
[56] II. Physikalisches Institut, Justus-Liebig-Universität Giessen, Giessen, Germany
[57] SUPA-School of Physics and Astronomy, University of Glasgow, Glasgow, UK
[58] LPSC, Université Grenoble Alpes, CNRS/IN2P3, Grenoble INP, Grenoble, France
[59] Laboratory for Particle Physics and Cosmology, Harvard University, Cambridge, MA, USA
[60] [(a)]Department of Modern Physics and State Key Laboratory of Particle Detection and Electronics, University of Science and Technology of China, Hefei, China; [(b)]Institute of Frontier and Interdisciplinary Science and Key Laboratory of Particle Physics and Particle Irradiation (MOE), Shandong University, Qingdao, China; [(c)]School of Physics and Astronomy, Shanghai Jiao Tong University, KLPPAC-MoE, SKLPPC, Shanghai, China; [(d)]Tsung-Dao Lee Institute, Shanghai, China
[61] [(a)]Kirchhoff-Institut für Physik, Ruprecht-Karls-Universität Heidelberg, Heidelberg, Germany; [(b)]Physikalisches Institut, Ruprecht-Karls-Universität Heidelberg, Heidelberg, Germany
[62] Faculty of Applied Information Science, Hiroshima Institute of Technology, Hiroshima, Japan
[63] [(a)]Department of Physics, Chinese University of Hong Kong, Shatin, N.T., Hong Kong, China; [(b)]Department of Physics, University of Hong Kong, Hong Kong, China; [(c)]Department of Physics and Institute for Advanced Study, Hong Kong University of Science and Technology, Clear Water Bay, Kowloon, Hong Kong, China
[64] Department of Physics, National Tsing Hua University, Hsinchu, Taiwan
[65] Department of Physics, Indiana University, Bloomington, IN, USA
[66] [(a)]INFN Gruppo Collegato di Udine, Sezione di Trieste, Udine, Italy; [(b)]ICTP, Trieste, Italy; [(c)]Dipartimento Politecnico di Ingegneria e Architettura, Università di Udine, Udine, Italy
[67] [(a)]INFN Sezione di Lecce, Lecce, Italy; [(b)]Dipartimento di Matematica e Fisica, Università del Salento, Lecce, Italy
[68] [(a)]INFN Sezione di Milano, Milan, Italy; [(b)]Dipartimento di Fisica, Università di Milano, Milan, Italy
[69] [(a)]INFN Sezione di Napoli, Naples, Italy; [(b)]Dipartimento di Fisica, Università di Napoli, Naples, Italy
[70] [(a)]INFN Sezione di Pavia, Pavia, Italy; [(b)]Dipartimento di Fisica, Università di Pavia, Pavia, Italy
[71] [(a)]INFN Sezione di Pisa, Pisa, Italy; [(b)]Dipartimento di Fisica E. Fermi, Università di Pisa, Pisa, Italy
[72] [(a)]INFN Sezione di Roma, Rome, Italy; [(b)]Dipartimento di Fisica, Sapienza Università di Roma, Rome, Italy
[73] [(a)]INFN Sezione di Roma Tor Vergata, Rome, Italy; [(b)]Dipartimento di Fisica, Università di Roma Tor Vergata, Rome, Italy
[74] [(a)]INFN Sezione di Roma Tre, Rome, Italy; [(b)]Dipartimento di Matematica e Fisica, Università Roma Tre, Rome, Italy
[75] [(a)]INFN-TIFPA, Trento, Italy; [(b)]Università degli Studi di Trento, Trento, Italy
[76] Institut für Astro- und Teilchenphysik, Leopold-Franzens-Universität, Innsbruck, Austria
[77] University of Iowa, Iowa City, IA, USA
[78] Department of Physics and Astronomy, Iowa State University, Ames, IA, USA
[79] Joint Institute for Nuclear Research, Dubna, Russia
[80] [(a)]Departamento de Engenharia Elétrica, Universidade Federal de Juiz de Fora (UFJF), Juiz de Fora, Brazil; [(b)]Universidade Federal do Rio De Janeiro COPPE/EE/IF, Rio de Janeiro, Brazil; [(c)]Universidade Federal de São João del Rei (UFSJ), São João del Rei, Brazil; [(d)]Instituto de Física, Universidade de São Paulo, São Paulo, Brazil
[81] KEK, High Energy Accelerator Research Organization, Tsukuba, Japan
[82] Graduate School of Science, Kobe University, Kobe, Japan
[83] [(a)]AGH University of Science and Technology Faculty of Physics and Applied Computer Science, Krakow, Poland; [(b)]Marian Smoluchowski Institute of Physics, Jagiellonian University, Krakow, Poland
[84] Institute of Nuclear Physics Polish Academy of Sciences, Krakow, Poland
[85] Faculty of Science, Kyoto University, Kyoto, Japan

[86] Kyoto University of Education, Kyoto, Japan
[87] Research Center for Advanced Particle Physics and Department of Physics, Kyushu University, Fukuoka , Japan
[88] Instituto de Física La Plata, Universidad Nacional de La Plata and CONICET, La Plata, Argentina
[89] Physics Department, Lancaster University, Lancaster, UK
[90] Oliver Lodge Laboratory, University of Liverpool, Liverpool, UK
[91] Department of Experimental Particle Physics, Jožef Stefan Institute and Department of Physics, University of Ljubljana, Ljubljana, Slovenia
[92] School of Physics and Astronomy, Queen Mary University of London, London, UK
[93] Department of Physics, Royal Holloway University of London, Egham, UK
[94] Department of Physics and Astronomy, University College London, London, UK
[95] Louisiana Tech University, Ruston, LA, USA
[96] Fysiska institutionen, Lunds universitet, Lund, Sweden
[97] Centre de Calcul de l'Institut National de Physique Nucléaire et de Physique des Particules (IN2P3), Villeurbanne, France
[98] Departamento de Física Teorica C-15 and CIAFF, Universidad Autónoma de Madrid, Madrid, Spain
[99] Institut für Physik, Universität Mainz, Mainz, Germany
[100] School of Physics and Astronomy, University of Manchester, Manchester, UK
[101] CPPM, Aix-Marseille Université, CNRS/IN2P3, Marseille, France
[102] Department of Physics, University of Massachusetts, Amherst, MA, USA
[103] Department of Physics, McGill University, Montreal, QC, Canada
[104] School of Physics, University of Melbourne, Melbourne, VIC, Australia
[105] Department of Physics, University of Michigan, Ann Arbor, MI, USA
[106] Department of Physics and Astronomy, Michigan State University, East Lansing, MI, USA
[107] B.I. Stepanov Institute of Physics, National Academy of Sciences of Belarus, Minsk, Belarus
[108] Research Institute for Nuclear Problems of Byelorussian State University, Minsk, Belarus
[109] Group of Particle Physics, University of Montreal, Montreal, QC, Canada
[110] P.N. Lebedev Physical Institute of the Russian Academy of Sciences, Moscow, Russia
[111] National Research Nuclear University MEPhI, Moscow, Russia
[112] D.V. Skobeltsyn Institute of Nuclear Physics, M.V. Lomonosov Moscow State University, Moscow, Russia
[113] Fakultät für Physik, Ludwig-Maximilians-Universität München, Munich, Germany
[114] Max-Planck-Institut für Physik (Werner-Heisenberg-Institut), Munich, Germany
[115] Nagasaki Institute of Applied Science, Nagasaki, Japan
[116] Graduate School of Science and Kobayashi-Maskawa Institute, Nagoya University, Nagoya, Japan
[117] Department of Physics and Astronomy, University of New Mexico, Albuquerque, NM, USA
[118] Institute for Mathematics, Astrophysics and Particle Physics, Radboud University Nijmegen/Nikhef, Nijmegen, The Netherlands
[119] Nikhef National Institute for Subatomic Physics and University of Amsterdam, Amsterdam, The Netherlands
[120] Department of Physics, Northern Illinois University, DeKalb, IL, USA
[121] [(a)] Budker Institute of Nuclear Physics and NSU, SB RAS, Novosibirsk, Russia; [(b)] Novosibirsk State University Novosibirsk, Novosibirsk, Russia
[122] Institute for High Energy Physics of the National Research Centre Kurchatov Institute, Protvino, Russia
[123] Institute for Theoretical and Experimental Physics named by A.I. Alikhanov of National Research Centre "Kurchatov Institute", Moscow, Russia
[124] Department of Physics, New York University, New York, NY, USA
[125] Ochanomizu University, Otsuka, Bunkyo-ku, Tokyo, Japan
[126] Ohio State University, Columbus, OH, USA
[127] Faculty of Science, Okayama University, Okayama, Japan
[128] Homer L. Dodge Department of Physics and Astronomy, University of Oklahoma, Norman, OK, USA
[129] Department of Physics, Oklahoma State University, Stillwater, OK, USA
[130] Palacký University, RCPTM, Joint Laboratory of Optics, Olomouc, Czech Republic
[131] Center for High Energy Physics, University of Oregon, Eugene, OR, USA
[132] LAL, Université Paris-Sud, CNRS/IN2P3, Université Paris-Saclay, Orsay, France
[133] Graduate School of Science, Osaka University, Osaka, Japan

[134] Department of Physics, University of Oslo, Oslo, Norway
[135] Department of Physics, Oxford University, Oxford, UK
[136] LPNHE, Sorbonne Université, Université de Paris, CNRS/IN2P3, Paris, France
[137] Department of Physics, University of Pennsylvania, Philadelphia, PA, USA
[138] Konstantinov Nuclear Physics Institute of National Research Centre "Kurchatov Institute", PNPI, St. Petersburg, Russia
[139] Department of Physics and Astronomy, University of Pittsburgh, Pittsburgh, PA, USA
[140] [(a)]Laboratório de Instrumentação e Física Experimental de Partículas - LIP, Lisbon, Portugal; [(b)]Departamento de Física, Faculdade de Ciências, Universidade de Lisboa, Lisbon, Portugal; [(c)]Departamento de Física, Universidade de Coimbra, Coimbra, Portugal; [(d)]Centro de Física Nuclear da Universidade de Lisboa, Lisbon, Portugal; [(e)]Departamento de Física, Universidade do Minho, Braga, Portugal; [(f)]Departamento de Física Teórica y del Cosmos, Universidad de Granada, Granada, Spain; [(g)]Dep Física and CEFITEC of Faculdade de Ciências e Tecnologia, Universidade Nova de Lisboa, Caparica, Portugal; [(h)]Instituto Superior Técnico, Universidade de Lisboa, Lisbon, Portugal
[141] Institute of Physics of the Czech Academy of Sciences, Prague, Czech Republic
[142] Czech Technical University in Prague, Prague, Czech Republic
[143] Charles University, Faculty of Mathematics and Physics, Prague, Czech Republic
[144] Particle Physics Department, Rutherford Appleton Laboratory, Didcot, UK
[145] IRFU, CEA, Université Paris-Saclay, Gif-sur-Yvette, France
[146] Santa Cruz Institute for Particle Physics, University of California Santa Cruz, Santa Cruz, CA, USA
[147] [(a)]Departamento de Física, Pontificia Universidad Católica de Chile, Santiago, Chile; [(b)]Universidad Andres Bello, Department of Physics, Santiago, Chile; [(c)]Departamento de Física, Universidad Técnica Federico Santa María, Valparaíso, Chile
[148] Department of Physics, University of Washington, Seattle, WA, USA
[149] Department of Physics and Astronomy, University of Sheffield, Sheffield, UK
[150] Department of Physics, Shinshu University, Nagano, Japan
[151] Department Physik, Universität Siegen, Siegen, Germany
[152] Department of Physics, Simon Fraser University, Burnaby, BC, Canada
[153] SLAC National Accelerator Laboratory, Stanford, CA, USA
[154] Physics Department, Royal Institute of Technology, Stockholm, Sweden
[155] Departments of Physics and Astronomy, Stony Brook University, Stony Brook, NY, USA
[156] Department of Physics and Astronomy, University of Sussex, Brighton, UK
[157] School of Physics, University of Sydney, Sydney, Australia
[158] Institute of Physics, Academia Sinica, Taipei, Taiwan
[159] [(a)]E. Andronikashvili Institute of Physics, Iv. Javakhishvili Tbilisi State University, Tbilisi, Georgia; [(b)]High Energy Physics Institute, Tbilisi State University, Tbilisi, Georgia
[160] Department of Physics, Technion, Israel Institute of Technology, Haifa, Israel
[161] Raymond and Beverly Sackler School of Physics and Astronomy, Tel Aviv University, Tel Aviv, Israel
[162] Department of Physics, Aristotle University of Thessaloniki, Thessaloniki, Greece
[163] International Center for Elementary Particle Physics and Department of Physics, University of Tokyo, Tokyo, Japan
[164] Graduate School of Science and Technology, Tokyo Metropolitan University, Tokyo, Japan
[165] Department of Physics, Tokyo Institute of Technology, Tokyo, Japan
[166] Tomsk State University, Tomsk, Russia
[167] Department of Physics, University of Toronto, Toronto, ON, Canada
[168] [(a)]TRIUMF, Vancouver, BC, Canada; [(b)]Department of Physics and Astronomy, York University, Toronto, ON, Canada
[169] Division of Physics and Tomonaga Center for the History of the Universe, Faculty of Pure and Applied Sciences, University of Tsukuba, Tsukuba, Japan
[170] Department of Physics and Astronomy, Tufts University, Medford, MA, USA
[171] Department of Physics and Astronomy, University of California Irvine, Irvine, CA, USA
[172] Department of Physics and Astronomy, University of Uppsala, Uppsala, Sweden
[173] Department of Physics, University of Illinois, Urbana, IL, USA
[174] Instituto de Física Corpuscular (IFIC), Centro Mixto Universidad de Valencia - CSIC, Valencia, Spain
[175] Department of Physics, University of British Columbia, Vancouver, BC, Canada
[176] Department of Physics and Astronomy, University of Victoria, Victoria, BC, Canada
[177] Fakultät für Physik und Astronomie, Julius-Maximilians-Universität Würzburg, Würzburg, Germany

[178] Department of Physics, University of Warwick, Coventry, UK
[179] Waseda University, Tokyo, Japan
[180] Department of Particle Physics, Weizmann Institute of Science, Rehovot, Israel
[181] Department of Physics, University of Wisconsin, Madison, WI, USA
[182] Fakultät für Mathematik und Naturwissenschaften, Fachgruppe Physik, Bergische Universität Wuppertal, Wuppertal, Germany
[183] Department of Physics, Yale University, New Haven, CT, USA

[a] Also at Borough of Manhattan Community College, City University of New York, New York, NY, USA
[b] Also at CERN, Geneva, Switzerland
[c] Also at CPPM, Aix-Marseille Université, CNRS/IN2P3, Marseille, France
[d] Also at Département de Physique Nucléaire et Corpusculaire, Université de Genève, Geneva, Switzerland
[e] Also at Departament de Fisica de la Universitat Autonoma de Barcelona, Barcelona, Spain
[f] Also at Department of Applied Physics and Astronomy, University of Sharjah, Sharjah, United Arab Emirates
[g] Also at Department of Financial and Management Engineering, University of the Aegean, Chios, Greece
[h] Also at Department of Physics and Astronomy, Michigan State University, East Lansing, MI, USA
[i] Also at Department of Physics and Astronomy, University of Louisville, Louisville, KY, USA
[j] Also at Department of Physics, Ben Gurion University of the Negev, Beer Sheva, Israel
[k] Also at Department of Physics, California State University, East Bay, USA
[l] Also at Department of Physics, California State University, Fresno, USA
[m] Also at Department of Physics, California State University, Sacramento, USA
[n] Also at Department of Physics, King's College London, London, UK
[o] Also at Department of Physics, St. Petersburg State Polytechnical University, St. Petersburg, Russia
[p] Also at Department of Physics, Stanford University, Stanford, CA, USA
[q] Also at Department of Physics, University of Adelaide, Adelaide, Australia
[r] Also at Department of Physics, University of Fribourg, Fribourg, Switzerland
[s] Also at Dipartimento di Matematica, Informatica e Fisica, Università di Udine, Udine, Italy
[t] Also at Faculty of Physics, M.V. Lomonosov Moscow State University, Moscow, Russia
[u] Also at Giresun University, Faculty of Engineering, Giresun, Turkey
[v] Also at Graduate School of Science, Osaka University, Osaka, Japan
[w] Also at Hellenic Open University, Patras, Greece
[x] Also at Institucio Catalana de Recerca i Estudis Avancats, ICREA, Barcelona, Spain
[y] Also at Institut für Experimentalphysik, Universität Hamburg, Hamburg, Germany
[z] Also at Institute for Mathematics, Astrophysics and Particle Physics, Radboud University Nijmegen/Nikhef, Nijmegen, The Netherlands
[aa] Also at Institute for Nuclear Research and Nuclear Energy (INRNE) of the Bulgarian Academy of Sciences, Sofia, Bulgaria
[ab] Also at Institute for Particle and Nuclear Physics, Wigner Research Centre for Physics, Budapest, Hungary
[ac] Also at Institute of Particle Physics (IPP), Vancouver, Canada
[ad] Also at Institute of Physics, Azerbaijan Academy of Sciences, Baku, Azerbaijan
[ae] Also at Instituto de Fisica Teorica, IFT-UAM/CSIC, Madrid, Spain
[af] Also at Joint Institute for Nuclear Research, Dubna, Russia
[ag] Also at LAL, Université Paris-Sud, CNRS/IN2P3, Université Paris-Saclay, Orsay, France
[ah] Also at Louisiana Tech University, Ruston, LA, USA
[ai] Also at Moscow Institute of Physics and Technology State University, Dolgoprudny, Russia
[aj] Also at National Research Nuclear University MEPhI, Moscow, Russia
[ak] Also at Physics Department, An-Najah National University, Nablus, Palestine
[al] Also at Physics Dept, University of South Africa, Pretoria, South Africa
[am] Also at Physikalisches Institut, Albert-Ludwigs-Universität Freiburg, Freiburg, Germany
[an] Also at The City College of New York, New York, NY, USA
[ao] Also at Tomsk State University, Tomsk, and Moscow Institute of Physics and Technology State University, Dolgoprudny, Russia

[ap] Also at TRIUMF, Vancouver, BC, Canada
[aq] Also at Universita di Napoli Parthenope, Naples, Italy
*Deceased